Contents lists available at ScienceDirect

Biosensors and Bioelectronics

journal homepage: http://ees.elsevier.com

Stretchable piezoelectric energy harvesters and self-powered sensors for wearable and implantable devices

Honglei Zhou [a,b], Yue Zhang [b,c], Ye Qiu [b,d], Huaping Wu [d], Weiyang Qin [a], Yabin Liao [e,***], Qingmin Yu [a,**], Huanyu Cheng [b,*]

[a] Department of Engineering Mechanics, School of Mechanics, Civil Engineering and Architecture, Northwestern Polytechnical University, Xi'an, 710129, China
[b] Department of Engineering Science and Mechanics, The Pennsylvania State University, University Park, PA, 16802, USA
[c] Department of Material Science, Fudan University, Shanghai, 200433, China
[d] Key Laboratory of E&M (Zhejiang University of Technology), Ministry of Education and Zhejiang Province, Hangzhou, 310014, China
[e] Department of Mechanical Engineering Technology, Pennsylvania State University-Erie, The Behrend College, Erie, PA, 16563, USA

ARTICLE INFO

Keywords
Stretchable piezoelectrics
Self-powered sensors
Piezoelectric energy harvesters
Wearable devices
Implantable devices

ABSTRACT

Wearable and implantable bio-integrated electronics have started to gain momentum because of their essential role in improving the quality of life for various patients and healthy individuals. However, their continuous operation is often limited by traditional battery technologies with a limited lifespan, creating a significant challenge for their development. Thus, it is highly desirable to harvest biomechanical energies from human motion for self-powered bio-integrated functional devices. Piezoelectric energy harvesters are ideal candidates to achieve this goal by converting biomechanical energy to electric energy. Because of their applications on soft and highly deformable tissues of the human body, these devices also need to be mechanically flexible and stretchable, thus posing a significant challenge. Effective methods to address the challenge include the exploration of new stretchable piezoelectric materials (e.g., hybrid composite material) and stretchable structures (e.g., buckled shapes, serpentine mesh layouts, kirigami designs, among others). This review presents an overview of the recent developments in new intrinsically stretchable piezoelectric materials and rigid inorganic piezoelectric materials with novel stretchable structures for flexible and stretchable piezoelectric sensors and energy harvesters. Following the discussion of theoretical modeling of the piezoelectric materials to convert mechanical deformations into electrical signals, the representative applications of stretchable piezoelectric materials and structures in wearable and implantable devices are briefly summarized. The present limitations and future research directions of flexible and stretchable piezoelectric devices are then discussed.

1. Introduction

The last few decades have witnessed the rapid development of wearable or bio-integrated devices due to their significant impacts on human health from preventative monitoring and early diagnostic confirmation to non-invasive and convenient therapeutic options (Cheng and Yi, 2017; Lou et al., 2020; Yi et al., 2019). As biological tissues and living organisms are intrinsically flexible and malleable, the successful integration of these biomedical devices on biological systems would require them to be bendable, foldable, twistable, and stretchable. Benefited from these characteristics, high-performance wearable and implantable devices have been rapidly developed to pliably conform to soft tissues. These demonstrated wearable and implanted biomedical devices include temperature sensors (Ren et al., 2016; Webb et al., 2013), sweat sensors (Gao et al., 2016; Zhang et al., 2020b), gas sensors (Yang et al., 2020; Yi et al., 2020), blood pressure sensors (Chun et al., 2018; Li et al., 2020a), glucose sensors (Chen et al., 2017b), heart rate monitors (Jeong et al., 2014; Yi et al., 2018), brain sensors (Kang et al., 2016), among others. Taken together, the expanded repertoire of sensors and devices opens up unprecedented opportunities for health monitoring. In addition to real-time and continuous monitoring of physiological and pathological parameters for informing disease conditions, they can also improve surgical procedures and therapeutic outcomes. Despite the rapid development in advanced battery technologies, their limited lifespan still requires replacement, which becomes even more challenging for implantable devices and poses health risks to patients (Liu et al. 2017a, 2018b; Wan et al., 2019; Xu et al., 2019; Zan et al., 2020). There-

* Corresponding author.
** Corresponding authors.
*** Corresponding author.
E-mail addresses: qingminyu@nwpu.edu.cn (Y. Liao); yul570@psu.edu (Q. Yu); Huanyu.Cheng@psu.edu (H. Cheng)

https://doi.org/10.1016/j.bios.2020.112569
Received 25 May 2020; Received in revised form 24 August 2020; Accepted 25 August 2020
Available online xxx
0956-5663/

fore, self-powered sensors and a sustainable power source for the bio-integrated devices are of vital interest (Chen et al. 2016, 2020; Meng et al., 2020; Su et al. 2020a, 2020b; Zhang et al., 2020a; Zhou et al. 2020b, 2020c).

Piezoelectric materials have been widely explored for self-powered sensors and energy harvesting solutions in bio-integrated devices because of their excellent capability to generate an electric charge in response to mechanical deformations. By leveraging the direct piezoelectric effect, piezoelectric energy harvesters (PEHs) or piezoelectric nanogenerators (PENGs) convert mechanical energy to electrical energy with high sensitivity, large power density, high durability, good scalability, and excellent mechanical stability, as well as simple design and easy operation. Typical designs involve the use of horizontal cantilevered beams or inverted beams (Lan et al., 2015; Pan et al., 2019) with one or two piezoelectric elements attached to the beam surface near the fixed end. Because these cantilevered beams are often associated with high natural resonance frequencies, the mechanical vibration energy in the vicinity of the structural frequency can be efficiently harvested. However, the frequency of human activity (<10 Hz) (Yan et al., 2020; Ylli et al., 2015) is much smaller than that of the PEHs. The energy conversion efficiency is, thus, significantly compromised, which renders a challenge to PEHs (Ma et al., 2016). Given this challenge, piezoelectric materials with improved performance and advanced structural designs have been proposed to efficiently harvest low-frequency vibration energies. For instance, the frequency up-conversion design (Fu and Yeatman, 2017; Kathpalia et al., 2017; Kuang et al., 2016; Pillatsch et al., 2014; Yeo et al., 2018) can convert the low-frequency vibration to higher frequency vibration through mechanical plucking or magnetic coupling.

The commonly used piezoelectric materials include piezoelectric polymers (e.g., polyvinylidene fluoride (PVDF) (Fu et al., 2018)), piezoelectric ceramics (e.g., $PbZr_xTi_{1-x}O_3$ (PZT), $BaTiO_3$ (BTO) (Kim et al., 2014), (K, Na)NbO_3 (Kang et al., 2015), and $ZnSnO_3$ (Guo et al., 2017)), piezoelectric inorganic semiconductors (e.g., GaN (Tsai et al., 2017), ZnO (Saravanakumar et al., 2013; Wang and Song, 2006; Yang et al., 2009), BiT (Abinnas et al., 2017), and InN (Ku et al., 2017)). It should be noted that organic/inorganic ferroelectric materials have also been widely used for piezoelectric devices (Owczarek et al., 2016; Yu et al., 2017a). The former piezoelectric polymers are flexible and can sustain relatively larger mechanical strains (~3% for PVDF (Qi and McAlpine, 2010)) than piezoceramic (~0.2% for PZT (Guillon et al., 2002)). However, the piezoelectric coefficient of piezoelectric polymers (20–30 pC/N for PVDF) is much lower than piezoelectric inorganic semiconductors and piezoceramic (250–700 pC/N for PZT) (Liu et al., 2018a). While the latter two inorganic piezoelectric materials are associated with relatively high piezoelectric coefficients, they are brittle and cannot withstand large deformations from the soft and highly deformable tissues of the human body. Therefore, it is of central research focus to develop stretchable piezoelectric energy harvesters and sensors with high piezoelectricity and large mechanical compliance (e.g., stretchability) (Yeo et al., 2018). To date, two classes of conceptually different strategies have been investigated for.

Stretchable piezoelectric devices: (1) intrinsically stretchable piezoelectric materials, and (2) stretchable structural designs. The former relies on advanced material synthesis, whereas the latter simply applies the stretchable structures (e.g., wavy/buckled geometries, fractal patterns, and kirigami layouts) to render stretchable properties in conventional brittle materials. Building on these two strategies, many flexible PEHs, and wearable sensors have been reported and applied for energy harvesting and health monitoring. However, novel piezoelectric materials and stretchable structures are still of high interest for combined improvement in both their mechanical and piezoelectric properties.

There have been a number of comprehensive reviews on the recent progress of PEHs, including materials, structures, methods, circuits and their applications in the biomedical field (Ali et al., 2019; Chorsi et al., 2019; Dagdeviren et al., 2016; Li et al., 2020d; Surmenev et al., 2019). However, stretchable PEHs and self-powered sensors with enhanced stretchability and piezoelectric properties enabled by advanced stretchable piezoelectric materials and novel stretchable structure designs have rarely been summarized. In this context, this review will highlight the recent advancement of stretchable piezoelectric devices with advanced stretchable piezoelectric materials and novel stretchable structures as self-powered sensors and energy harvests for wearable and implantable electronics (Fig. 1). We will first introduce the fundamental of the PEHs in Section 2. Next, we introduce the intrinsically stretchable piezoelectric materials in Section 3, and discuss various stretchable structures to render the relatively rigid, inorganic piezoelectric materials stretchable in Section 4. Stretchable electrodes and manufacturing techniques for stretchable piezoelectric devices are presented in Section 5 and Section 6, respectively. The modeling efforts of stretchable PEHs and self-powered sensors based on buckled structures are briefly summarized in Section 7. Because of the combined enhancement in their piezoelectric performance and mechanical compliance realized by novel structures and advanced materials, Section 8 presents several representative applications of flexible and stretchable PEHs and self-powered sensors in wearable and implantable devices. Lastly, the conclusion is drawn, and perspectives are provided to highlight a small fraction of opportunities for future development.

2. Fundamental of piezoelectric energy harvester

First discovered by the Pierre and Jacques Curie brothers in 1880 and named by Hankel in 1881, piezoelectricity depicts the interaction between mechanical and electrical states, including the *direct piezoelectric effect* and *converse piezoelectric effect*. In the former, the piezoelectric material can generate an electric charge when mechanical strain is applied, which has mainly been used in energy harvesting and structural sensing. Conversely, the latter converts the electric power to a mechanical strain for actuation and active vibration controls of mechanical structures and systems (Wei and Jing, 2017). A simple molecular model can be used to explain the underlying mechanism of the electric charge generation under external stresses for the *direct piezoelectric effect*, which is the main focus in this review (Sun et al., 2020b). The gravity centers of the positive and negative charges of each molecule coincide under a strain-free state, resulting in an electrically neutral molecule. When exerting external stress on the piezoelectric material, the deformation of the internal molecular structure causes the separation of the negative and positive gravity centers of the molecules and further generation of little dipoles. As a result, the material is polarized with the charge only on the surfaces as the facing poles inside the material are canceled. An electric field is generated by this polarization and mechanical energy, therefore, can be transformed into electrical energy.

Based on the *direct piezoelectric effect*, various PEHs are designed and fabricated by depositing two electrodes on both the front and back of the piezoelectric materials. When two electrodes are connected through a wire or load, a flow of free charges driven by the generated electric field is then produced. This flow of free charges between the two electrodes remains until the free charge neutralizes the polarization effect. After the external mechanical force is removed, free charges flow back to their initial positions due to the disappearance of the polarization. Under the periodical variation of external strain, the PEHs can generate an alternating current output. There are two common working modes for the PEHs, i.e. “33” mode and “31” mode, with the poling axis coincident with the mechanical strain axis in the former and mutually perpendicular in the latter (Wei and Jing, 2017).

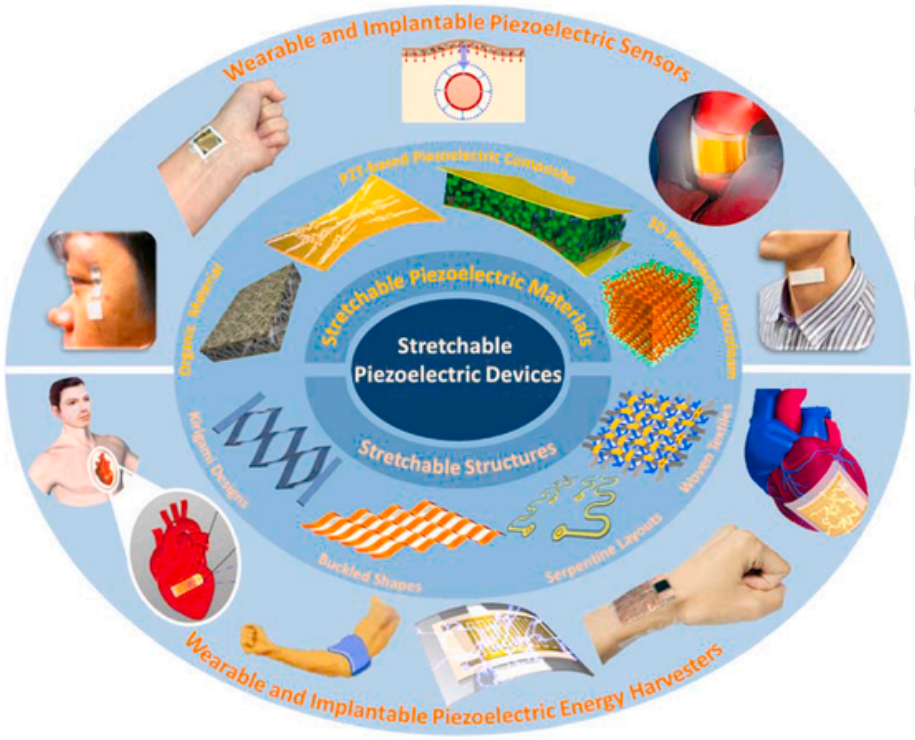

Fig. 1. Stretchable piezoelectric sensors and energy harvesters for wearable and implantable electronics. The enhanced stretchability and piezoelectrics properties are enabled by advanced stretchable piezoelectric materials and novel stretchable structural designs. Advanced stretchable piezoelectric materials include 1) organic piezoelectric materials (Maity and Mandal, 2018); Copyright 2018, American Chemical Society; 2) piezoelectric composite (Chou et al., 2018; Niu et al., 2019); Copyright 2018, Elsevier Ltd; Copyright 2019, American Chemical Society; 3) 3D piezoelectric microfoam (Zhang et al., 2018a); Copyright 2018, The Royal Society of Chemistry. Novel stretchable structural designs include 1) buckled shapes (Qi et al., 2011); Copyright 2011, American Chemical Society; 2) serpentine layouts (Ji et al., 2020); Copyright 2020, Elsevier Ltd; 3) kirigami designs (Zhou et al., 2020a); 4) woven textiles (Ahn et al., 2015b); Copyright 2015, IOP Publishing Ltd. These devices are used to harvest energy from heartbeat (Jeong et al., 2017; Sun et al., 2019); Copyright 2019, WILEY-VCH Verlag GmbH & Co., KGaA, Weinheim, wrist (He et al., 2019); Copyright 2018, American Chemical Society, arm (Mondal et al., 2020); Copyright 2020, Elsevier Ltd, and other human motions. Furthermore, they have been explored as self-powered sensors to monitor blood pressure (Cheng et al., 2016); Copyright 2015, Elsevier Ltd, pulse (Park et al., 2016); Copyright 2016, American Chemical Society, and skin/muscle movements (Hu and Wang, 2015; Liu et al., 2017b); Copyright 2015, Elsevier Ltd; Copyright 2017, IOP Publishing Ltd.

3. Stretchable piezoelectric materials

Common stretchable piezoelectric materials include intrinsic piezoelectric materials and piezoelectric electret. The former is best represented by piezoelectric polymers, including PVDF, polyvinylidene fluoride-trifluoroethylene P(VDF-TrFE), and odd nylon. While the materials themselves in the latter are not piezoelectric, the process of high-voltage polarization leads to the gas breakdown in the materials to form an electric dipole, exhibiting piezoelectric effects in the process of material compression. Because of dipoles and ionic groups in biomacromolecules, many biological tissues such as collagen fiber and DNA also have piezoelectric properties (i.e., biopiezoelectricity). The action of stress rotationally polarizes these tissues to induce macroscopic polarized charge; under the action of an electric field, their structural strain changes as well. Because piezoelectric materials are the essential components in piezoelectric energy harvesters and sensors, they play a crucial role in improving the output of energy harvesters and the sensitivity of sensors. This section will focus on stretchable piezoelectric materials and their functional composites to achieve high piezoelectric performance and stretchable properties.

3.1. Piezoelectric polymers and their composites

Initial exploration of flexible self-powered sensors and energy harvesters has nucleated around piezoelectric polymers due to their good flexibility and excellent biocompatibility. However, the applications are limited by their low piezoelectric coefficients. Incorporating various piezoelectric fillers into the piezoelectric polymer matrices represents a simple method to improve their piezoelectric properties, owing to the simplicity and cost-effectiveness of this method (Kar et al., 2019). It should be noted that although the α-phase in the PVDF is its dominant crystalline phase, only its oriented polar β phases have piezoelectric effects. Thus, methods to achieve a higher content of polar phases have been sought after. As P(VDF-TrFE) has a higher content of the β phase, it is commonly explored over its PVDF counterparts. Meanwhile, the transformation from the α-phase to polar β-phase in the piezoelectric polymers can also be promoted by using fillers, including ZnO (Dahiya et al., 2018; Li et al., 2019b; Parangusan et al. 2018a, 2018b), Al_2O_3 (Li et al., 2019a), Ag nanoparticles (NPs) (Almusallam et al., 2017; Issa et al., 2017), 2D SnO_2 nanosheet (Kar et al., 2019), and graphene (El Achaby et al., 2012).

Although the piezoelectric composite materials have enhanced piezoelectric properties, the large difference in the dielectric constant between the inorganic piezoelectric ceramic and polymer matrix often results in highly inhomogeneous electric fields during the polarization process. Therefore, the breakdown strength of the composites significantly reduces. One method to address this challenge is to explore the fillers (e.g., MgO NPs) with a similar dielectric constant of the polymer matrix (e.g., PVDF) (Singh et al., 2018). Besides the increased breakdown strength, the MgO also plays a vital role in imparting low leakage currents (Lim et al., 2006).

3.2. Inorganic piezoelectric nanomaterials in the polymeric matrix

As the piezoelectric properties of the fillers could overweigh that of the matrix, the matrix is no longer needed to be limited to piezoelectric polymers. Exploring stretchable non-piezopolymers as the matrix in the piezoelectric composites can further enhance their mechanical compliance. The composites typically comprise inorganic fillers with high piezoelectricity and polymer matrix with excellent stretchability. The commonly used piezoelectric fillers include BTO (Choi et al., 2016; Yan and Jeong, 2016), PZT (Hou et al., 2020; Liu et al., 2019a), and (1-*x*)Pb(Mg, Nb)$O_{3-x}PbTiO_3$ (PMN-PT) (Das et al., 2018; Hwang et al., 2014; Jeong et al., 2015; Xu et al., 2013). The diverse matrix materials range from low-cost silicone rubber (Choi et al., 2017) (e.g., polydimethylsiloxane (PDMS) (Sultana et al., 2015) or Ecoflex) to their composites (e.g., PDMS-carbon nanotubes (CNTs)).

For instance, the dispersion of PZT particles in the silicone rubber yields a stretchable piezoelectric nanogenerator (SPENG) (Fig. 2A) (Chou et al., 2018). Incorporating Ag-coated glass microspheres into the identical polymer matrix yields the corresponding flexible electrode, which helps substantially increase the contact area and quality to the piezoelectric layer because of the use of the same polymer matrix. The resistance of the SPENG is relatively stable during the stretching-releasing processes with a tensile strain of up to 100%. Similarly, well dispersing and blending PMN-PT particles and multi-walled CNTs (MWCNTs) in the Ecoflex silicone elastomer result in a piezoelectric elastic composite (Fig. 2B) (Jeong et al., 2015). Because the Ecoflex has a lower Young's modulus than that of the PDMS, the resulting stretchable elastic-composite generator can be stretched over 200% without mechanical cracking or delamination. The generated voltage and current under a 200% stretching strain can reach up to 4 V and 500 nA.

3.3. Three-dimensional microstructured piezoelectric materials

The structural design of piezoelectric materials is an efficient mechanism to improve their piezoelectricity and mechanical compliance. Thus, efforts have been attempted to introduce various three-dimensional (3D) microstructures in the piezoelectric materials. Among diverse 3D microstructures, the hemisphere and pyramid have been shown to enhance the piezoelectric performance (Lee et al., 2015; Mao et al., 2014; Park et al., 2015). Piezoelectric materials with microstructured surfaces have a substantial variation in the strain along with the.

thickness of the film compared to their flat counterparts, producing a much higher electrical output under the external impact. Because microstructured surfaces only lead to localized strain increase, porous structures within the entire piezoelectric film are reported to further improve the piezoelectric performance. Having a smaller Young's modulus, the porous film can also achieve high compressibility for generating higher output voltage and current.

Although the aforementioned works enhance the piezoelectric performance, their improvement in the stretchability of devices is limited. The relatively low stretchability of piezoelectric sensors and en-

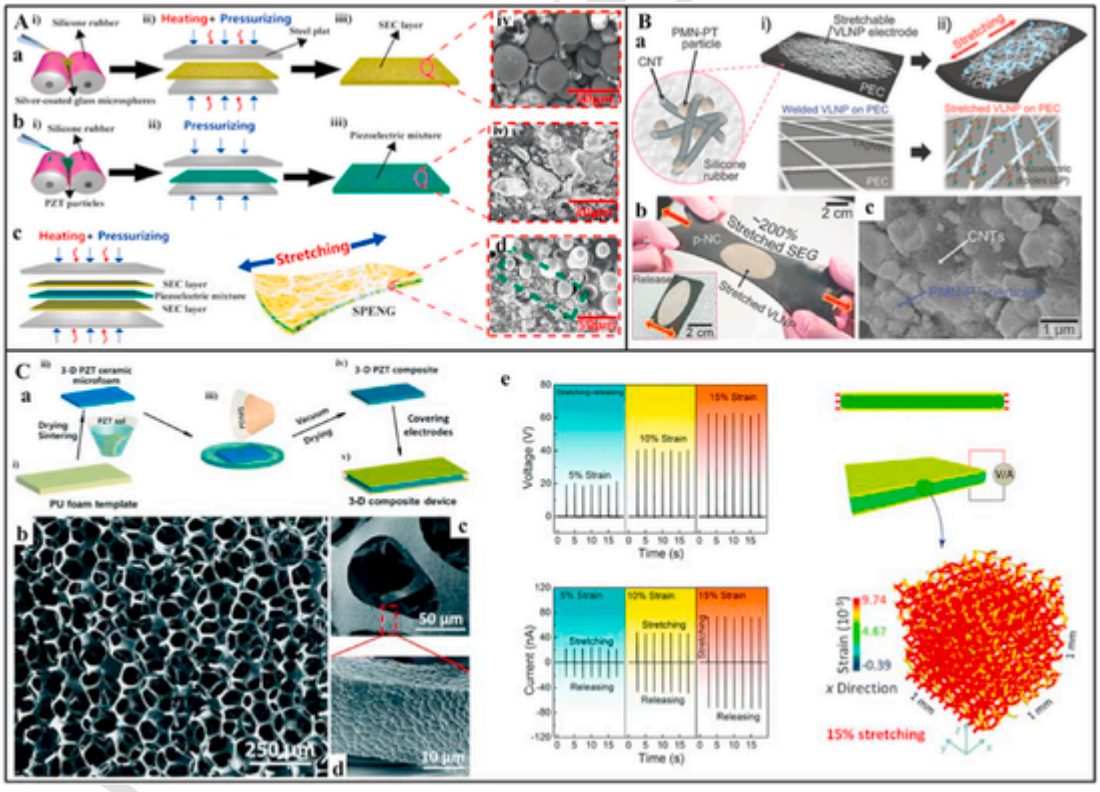

Fig. 2. Stretchable piezoelectric materials and their functional composites. (**A**) Stretchable PEH based on PZT particles and Ag-coated glass microspheres fillers. Fabrication processes of (a) stretchable electrode composite (SEC) layer, (b) stretchable piezoelectric composite (SPC) layer, and (c) stretchable piezoelectric PEH. (d) The SEM image of the PEH cross-sectional view. Reproduced with permission from (Chou et al., 2018); Copyright 2018, Elsevier Ltd. (**B**) Hyper-stretchable elastic-composite generator based on nanocomposite, with (a) a schematic illustration to show rubber-based piezoelectric elastic composite and long nanowires (NWs) percolation (VLNP) electrodes. (b) The final stretchable elastic-composite generator that is stretched by human hands. (c) An SEM image of the well-dispersed nanomaterials consisting of PMN-PT microparticles and MWCNTs. Reproduced with permission from (Jeong et al., 2015); Copyright 2015, WILEY-VCH Verlag GmbH & Co., KGaA, Weinheim. (**C**) Stretchable energy harvester based on 3-D PZT polymer composites. (a) Schematics of the preparation procedure. (b) The SEM image of the 3-D PZT ceramic microfoams. (c) The magnified SEM image of the PZT skeletons. (d) The localized surface morphology of the skeleton. (e) Output voltage and current of the 3-D composites under compression with different compressive strains. Reproduced with permission from (Zhang et al., 2018a); Copyright 2018, The Royal Society of Chemistry.

ergy harvesters limits their realistic application in the biomedical field. Exploiting 3D cellular-structured PZT ceramic foam filled with PDMS yields an intrinsically stretchable piezoelectric composite with enhanced stretchability while maintaining excellent piezoelectric properties (Zhang et al., 2018a). The resulting stretchable energy harvester based on the 3D composite produces a highly stable output voltage under a tensile strain of 15% (Fig. 2C). Compared with ceramic-polymer composites with embedded low-dimensional ceramic fillers, the interconnected 3D structure provides a continuous pathway for load transfer, which explains the superior piezoelectric properties. This method effectively solves the problem of poor load-transfer efficiency that typically scales with the stiffness ratio of the polymer matrix to the ceramic fillers.

3.4. Multilayer structured piezoelectric materials

The design of piezoelectric materials with a multilayer structure is also an effective way to improve piezoelectric properties. The double-layered piezoelectric film exhibits an improved piezoelectric output, which is attributed to the electric capacity enhancement of the double-layered structure (Hu et al., 2018b). In the single-layered piezoelectric film, the electric charge induced by external stimuli can only be stored at the interface between the film and the electrodes. In the double-layered piezoelectric film, the charges accumulated at the additional interlayer interface between two piezoelectric layers contribute to the enhanced capacitance of the film. Thus, the piezoelectric with a double-layered structure produces more free charge carriers to balance the higher internal piezoelectric potential through the external circuit to improve the piezoelectric output. Besides, the structural design of piezoelectric films with a triple-multilayer interlocked micro-dome geometry shows great potential in flexible electronics (Lee et al., 2018b). Higher piezoelectric performance is obtained because of the stress concentration between interlocked micro-dome arrays and increased contact area in the multilayer design.

In summary, various stretchable piezoelectric polymers have been synthesized and demonstrated for flexible and stretchable piezoelectric sensors and energy harvesters. In addition to superior stretchable properties, their piezoelectric properties are also enhanced. The stretchable and piezoelectric properties of various stretchable piezoelectric polymers/composites as energy harvesters are summarized and compared in Table 1.

4. Inorganic piezoelectric materials with stretchable structures

While inorganic piezoelectric/ferroelectric materials are not intrinsically stretchable, novel stretchable structures of their thin films have been explored to render them stretchable (Xue et al., 2020). The commonly explored stretchable structures include wavy/buckled geometries (Ding et al., 2015; Dong et al., 2019a; Feng et al., 2011; Han et al., 2019; Lagomarsini et al., 2019; Qi et al., 2011; Su et al., 2015b), serpentine layouts (Li et al., 2019c; Su et al., 2017; Yan et al., 2019b), fractal patterns (Duan et al., 2017), kirigami layouts (Isobe and Okumura, 2016; Lyu et al., 2017; Rafsanjani and Bertoldi, 2017; Shyu et al., 2015; Sun et al., 2020a; Wang et al., 2017), helical structures (Kim and Yun, 2017), and woven textiles (Ahn et al., 2015b; Baniasadi et al., 2015; Gong et al., 2020; Gutruf et al., 2019; Kim et al., 2017; Lund et al., 2018; Song and Yun, 2015; Zhang et al., 2015b; Zhou et al., 2017). The high-performance inorganic piezoelectric materials with these novel structures can endure much larger mechanical deformation while retaining high piezoelectricity. In this section, the progress of the high-performance stretchable sensors and PEHs with various stretchable structures is briefly summarized.

4.1. Buckled structures

The wavy or buckled structures can withstand large mechanical deformations by reducing their buckling amplitude and increasing wavelength. The pre-strain strategy has been widely used for the formation of buckled structures (Zhang et al., 2019b). Because buckled piezoelectric ribbons fabricated on flexible thin films can maintain high piezoelectricity, they have been widely applied in the structural design of stretchable PEHs. For instance, arrays of out-of-plane buckled PZT ribbons have been fabricated on flexible substrates (Fig. 3A) (Qi et al., 2011). In addition to the stretchable properties enabled by the buckled structures, the piezoelectric coefficients of the PZT ribbon before and after poling have been enhanced (i.e., 80 and 130 p.m./V in the buckled regions as compared to 40 and 75 p.m./V in the flat regions). The enhancement is attributed to the strain gradient created in the buckled PZT ribbons. The positive (or negative) maximum strain gradient occurs at the peak (or trough) locations in the buckled PZT ribbons, whereas it is vanishing in the flat regions. With the piezoelectric enhancement from the large, position-dependent strain gradient, buckled PZT ribbons provide promising applications for stretchable PEHs and self-powered piezoelectric sensors.

4.2. Serpentine structures and self-similar designs

The same ZnO nanoribbons have also been configured into serpentine ZnO nanoribbons bonded on a soft substrate via anchors (Ma et al., 2013). Similarly, the serpentine structure can also be applied to piezoelectric polymers such as PVDF to provide improved stretchable property. As a representative example, the stretchable micromotion sensor based on piezoelectric PVDF thin film in a serpentine layout can be stretched to 27.5% with high sensitivity of 72V/ε and 272.73 nA/ε (Fig. 3B) (Yan et al., 2019a). Integrating the micromotion sensor with a baseball cap provides a device that can successfully monitor the lower jaw (or throat) movement for speech pattern recognition. In addition to direct patterning, the serpentine structures can also be created by in-plane buckling behaviors (Ding et al., 2015) (Fig. 3C). The fabricated stretchable PVDF nanofibers with in-plane buckled structures can be stretched over 100%. Under the stretching-releasing cycle with 30% strain at a frequency of 0.5 Hz, a device consisting of ca. 120 in-plane buckled PVDF fibers can generate a voltage of 40 mV and a current of 1.2 nA.

Further enhancement in the mechanical deformation capabilities (e.g., stretchability, bendability, foldability, and twistability) can be realized by exploiting fractal design layouts. The device with a fractal serpentine structure can be stretched to 200% with maximum output currents up to 150 nA during the stretching-releasing process at a frequency of 4Hz (Fig. 3D) (Duan et al., 2017; Huang et al., 2017). The application of these stretchable structures can also go beyond the demonstrated PVDF fibers to the other high-performance piezoelectric materials to harvest the low-frequency mechanical energy from human motions.

Because of improved bandwidth and frequency tunability (Han et al., 2019; Ning et al. 2017, 2018b), sophisticated 3D piezoelectric microsystems with extended operation modes have been explored for enhanced energy harvesting (Fig. 3E). These 3D mesostructures with ultralow-stiffness piezoelectric materials can provide complex vibration-induced modes of motion. Another advantage of the 3D structure is the broadband operation for energy harvesting. The 3D buckled structure with a serpentine PVDF ribbon and a proof (Cu, 500 μm × 500 μm × 500 μm) can generate electrical power within a wide range of frequencies from 5 Hz to 500 Hz under out-of-plane vibrations with accelerations from 4 g to 0. In this case, the buckled shape provides two stable states during vibrations, and the serpen-

Table 1
Performance comparison of stretchable PEHs based on piezoelectric polymers or composites.

Materials	Key process	Form	Electrodes	Poling	Stretchability	Excitation	Output Voltage	Output Current	Power Density	Reference
Barium titanate NPs-polyurethane, P(VDF-TrFE), PDMS	Electrospinning	Composite nanofibers mat	Graphite	No	40%	40% Stretching strain (SS)	9.3 V	189 nA	1.76 μW/cm ^{2}	Siddiqui et al. (2018)
P(VDF-TrFE)	Electrospinning (400 rpm) annealing	Fiber	Al, indium tin oxide (ITO)	No	7%	Bending 15 mm (Radius)	/	/	1.35 mW/cm ^{3}	Kim et al. (2019a)
samarium-doped PMN-PT, PDMS	Sintering + freeze-drying	3D Composite foam	Ag	Yes	45%	35 N, compressive force (CF)	60 V	850 nA/cm ^{2}	11.5 μW/cm ^{2}	Zhang et al. (2018b)
3D PZT, PDMS	Sintering,	3D Composite foam	Metal	Yes	15%	15% (SS)	65 V	75 nA	/	Zhang et al. (2018a)
PZT, silicone rubber (SR)	Heating + pressurizing	Composite thin film	composite electrode (CE)	Yes	50%	50% (SS), 0.7 Hz	20 V	0.55 μA	3.93 μW/cm ^{3}	Chou et al. (2018)
PZT, polysiloxane matrix	Heating + pressurizing	Composite thin film	CE	Yes	50%	50% (SS), 0.7 Hz	8 V	0.4 μA	/	Qian et al. (2019)
PZT, Cu–Ag nanofibers, SR	Dispersing + curing	Composite thin film	CE	Yes	50%	50% (SS), 0.7 Hz	61 V	1.1 μA	/	Zhu et al. (2019)
PZT, SR	Mixing	Composite thin film	CE	Yes	30%	30% (SS), 6.25 cm/s	35 V	0.5 μA	81.2 μW/cm ^{3}	Niu et al. (2019)
P(VDF-TrFE)	Electrospinning	Fiber	Silver-coated nylon, CNTs	No	5%	5% (SS), 40 Hz	0.47 V	/	0.44 μW/cm ^{3}	Sim et al. (2015)
boron nitride nanosheet, PVDF	Electrospinning	Composite membranes	Al	No	~110%	10N (CF), 1 Hz	0.9 V	0.5 μA	/	Zhang et al. (2019a)
P(VDF-TrFE), PDMS	Dip coating + Spraying	Hollow fiber	MWCNTs,	Yes	100%	50% (SS), 50 cm/s	0.9 V	5 nA	/	Ryu et al. (2019)
ZnO, PDMS	Depositing	Composite thin film	Au	No	8%	8% (SS), 1 Hz	2 V	/	1.27 mW/cm ^{2}	Voiculescu et al. (2019)
ZnO, PDMS	Sputtering	Composite thin film	ITO/polyethylene terephthalate (PET)	No	40%	0.425% (SS)	6 V	/	0.2 μW/cm ^{2}	Chun et al. (2015)
PMN-PT, MWCNTs, PVDF	Heating + sintering	Composite thin film	Ag	No	6%	finger tapping	3–4 V	30–35 nA	/	Das et al. (2018)

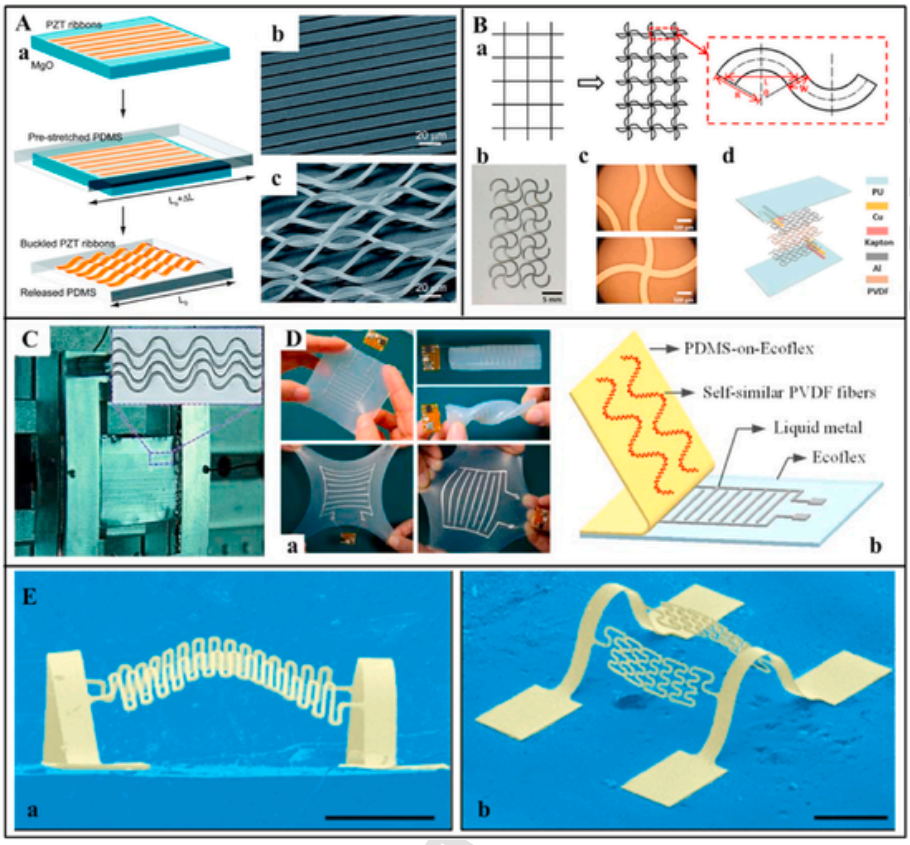

Fig. 3. Stretchable piezoelectric harvesters and sensors realized by bucked, serpentine, and fractal structures. (**A**) Buckled PZT ribbons for stretchable PEHs. (a) The schematic formation process of wavy/buckled piezoelectric PZT ribbons. SEM images of PZT ribbons transfer printed onto the PDMS (b) without pre-strain or (c) after the release of the pre-strain. Reproduced with permission from (Qi et al., 2011); Copyright 2011, American Chemical Society. (**B**) Stretchable sensor based on serpentine structure. (a) Schematic of the serpentine layout. (b) Photograph and (c) optical images of the PVDF film in a serpentine layout. (d) Exploded view of the micro-motion stretchable sensor with a serpentine layout. Reproduced with permission from (Yan et al., 2019a); Copyright 2019, American Chemical Society. (**C**) Photograph of the stretchable PEH based on in-plane buckled fibers. Reproduced with permission from (Ding et al., 2015); Copyright 2015, WILEY-VCH Verlag GmbH & Co., KGaA, Weinheim. (**D**) Ultra-stretchable PEH based on a fractal structure with aligned nanofibers. (a) Photographs of the flexible PEH under various deformations, including bending, twisting, and uniaxial/biaxial stretching. (b) The schematic diagram of the stretchable PEH comprises PDMS and Ecoflex layer, self-similar PVDF fibers, and liquid metal. Reproduced with permission from (Duan et al., 2017). (**E**) Stretchable 3D PVDF piezoelectric structure with (a) first-order and (b) second-order fractal curves. Reproduced with permission from (Han et al., 2019); Copyright 2019, Springer Nature.

tine layout reduces the energy barrier between these two states, thereby facilitating the excitation of nonlinear vibrational responses. Furthermore, the 3D buckled serpentine structure generates a notably larger output voltage than that of the 2D serpentine over a wide range of frequencies. Therefore, this class of 3D PEHs with serpentine layout clearly offers excellent mechanical properties, including low resonant frequency, wide bandwidth, and large-amplitude vibrations. A system with these features can efficiently harvest energies from low-frequency vibrations, such as human motions (with a frequency lower 10 Hz) or machine-induced vibrations (with a frequency of 10–100 Hz).

4.3. Kirigami designs

The kirigami approach has expanded the design diversity for a wide range of piezoelectric materials from nanoscale to microscale. Creating a kirigami pattern in the functional nanocomposites can dramatically increase the compliance of the materials and their stretchability from 2% to 300% with little compromise in their functional performance (Hu et al., 2018a; Kunin et al., 2016; Lamoureux et al., 2015; Lyu et al., 2017; Ning et al., 2018a; Song et al., 2015; Sun et al., 2019; Tang et al., 2017; Wang et al., 2017; Xu et al., 2017). Several kirigami structures with simple linear patterns (Fig. 4A and B), fractal-cut patterns, and T-joint-cut kirigami structures (Fig. 4C) are presented. Introducing linear cut patterns in the PVDF thin film on a PET soft substrate leads to a stretchable piezoelectric sensor system (Fig. 4A). Although there is a small reduction in piezoelectric performance for the thin film with linear cut patterns compared to that without cuts, its output voltage can still reach 1.63 V under the stretch/release cycles with a tensile strain of 10% at a frequency of 10 Hz (Sun et al., 2018). Two different interdigitated patterned cuts in PVDF films are also created: (1) center-cutting design with center cuts of 10 mm and edge cuts of 5 mm in length, and (2) edge cutting design that only has 10-mm-long cuts along the edge (Hu et al., 2018a) (Fig. 4B). The measurement results indicate the two resulting kirigami-based PVDF films attain a slightly smaller output voltage (i.e., 132 mV for center-cutting design and 85 mV for edge-cutting patter) compared to the film without cuts of 160 mV. However, the kirigami structures allow the PVDF films to attain a much higher stretchability of 18% than that without cuts of only 1%. The output voltage mainly depends on the stress distribution induced by the in-plane stretching of the film. The PVDF film with the center-cutting design has a larger portion of surface area under.

tensile stress upon stretching, thereby generating a higher output voltage. Further improvements in the output voltage can be possible by modulating the deformation of the center-cutting design. One effective solution is to explore fractal-cut kirigami structures, as shown in the middle of Fig. 4C (Kunin et al., 2016). By introducing perpendicular cuts on each end of the long cutting, the design has increased compliance, but the piezoelectric performance of the resulting structure is just slightly better than the simple kirigami structure. This is because

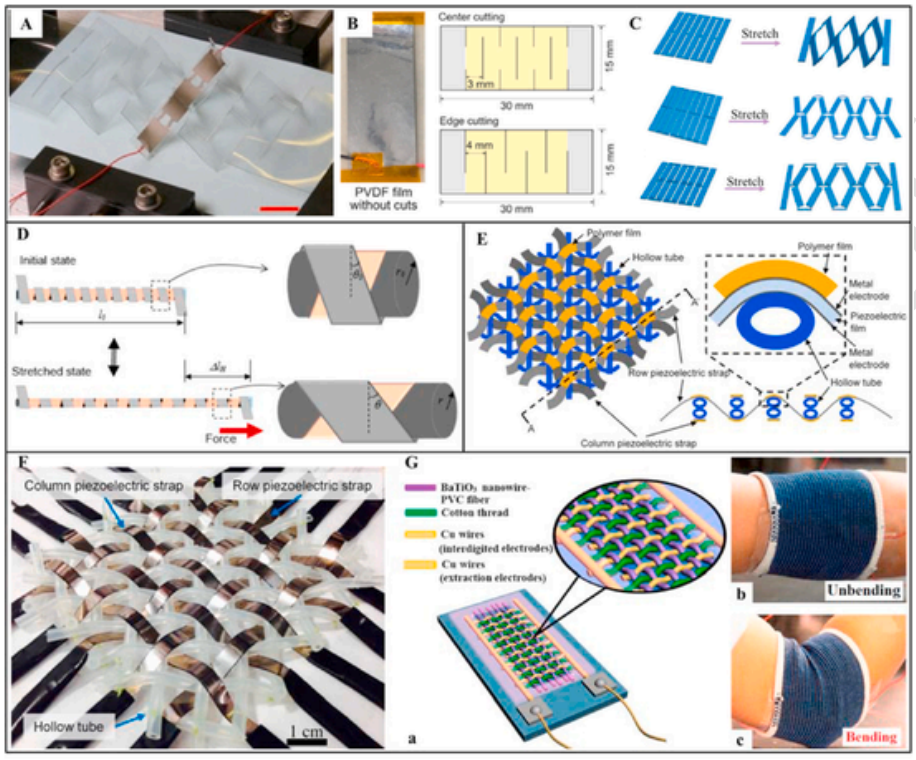

Fig. 4. Stretchable piezoelectric energy harvesters realized by kirigami, helical and woven structures. (**A**) Photographs of the PVDF-based stretchable piezoelectric sensor realized by simple kirigami structure. Reproduced with permission from (Sun et al., 2018). (**B**) The design of the PVDF films with center-cutting and edge-cutting kirigami patterns. Reproduced with permission from (Hu et al., 2018a); Copyright 2018, American Physical Society. (**C**) Three different designs of kirigami structures and corresponding stretching modes: simple kirigami structure, fractal-cut kirigami structure, and T-joint-cut kirigami structure. Reproduced with permission from (Zhou et al., 2020a). (**D**) Schematic of stretchable helical PEH with the outer PVDF strap and inner fabric band forming two helical structures in counter directions around the elastic core. Reproduced with permission from (Kim and Yun, 2017). (**E**) Schematic of the self-powered stretchable piezoelectric sensor based on woven structure and cross-sectional views. (**F**) Photograph of the fabricated prototype device based on woven piezoelectric straps. Reproduced with permission from (Ahn et al., 2015b); Copyright 2015, IOP publishing Ltd. (**G**) (a) Schematic diagram of the flexible fiber-based piezoelectric PEH. The deigned harvester is attached on an elbow pad to harvest the biomechanical energy during the (b) unbending and (c) bending process induced by the human arm. Reproduced with permission from (Zhang et al., 2015b); Copyright 2015, Elsevier Ltd.

the perpendicular cuttings can only be opened by the in-plane perpendicular force. A novel T-joint-cut kirigami structure at the bottom of Fig. 4C has then been proposed to overcome this limitation, where short cuttings in the perpendicular direction connect to the long cuttings at the ends (Zhou et al., 2020a). This new kirigami design not only helps avoid out-of-plane deformation but also further improves the stretchability to ~300% due to the enhanced in-plane rotation. Research shows that the T-joint-cut kirigami structure has the largest in-plane displacement, which is 6.3 times of the simple kirigami structure and 5.5 times of that with a fractal-cut pattern, respectively. The strain in the T-joint-cut kirigami structure is also 1.63 times and 1.45 times of the fractal-cut and simple kirigami structures. As the stretchability leads to in-plane rotation about the joints, its effect on the output voltage is minimal. No significant variation is observed in the output voltage (6 V) and power density (1.4 $\mu W/cm^2$ for a load resistance of 10 MΩ), as the sample is stretched from 0 to 300% by a force of 60 N at a frequency of 5 Hz.

4.4. Helical structures

Highly stretchable PEHs and sensors can also be realized by exploring helical structures. Fig. 4D presents a highly stretchable PVDF-based helical PEH by twining polymer PVDF strap and fabric band around the elastic core in counter directions to form two helical structures (Kim and Yun, 2017). Besides a highly stretchable property up to 158%, the fabricated PEH can also be stitched on the surface of garments to harvest mechanical energy generated from general human motions. The stretching applied on the helical PEH leads to torsional stress and longitudinal tensile stress owing to the helical structure, which produces alternating potential in the helical PVDF strap during the periodic stretching-releasing motions. For a loading frequency of 1 Hz and a load resistance of 3 MΩ, the helical PEH generates a maximum output power and power density up to 1.42 mW and 296 $\mu W/cm^2$, respectively. Applying the helical PEH on the knee generates a peak-to-peak output voltage larger than 20 V during bending motion and 4 V during squat motion.

4.5. Woven textiles

The woven textile provides another feasible solution for wearable and flexible PEHs and sensing systems with high stretchability because of its capability to follow complex mechanical deformations (Dong et al., 2020). The most common method is to weave the threads (e.g., yarn string) and piezoelectric film straps together for fabricating textile-based PEHs. As a representative example, a flexible and wearable self-powered tactile sensor array is fabricated by weaving the piezoelectric straps, polymer films, and elastic hollow tubes together (Fig. 4E) (Ahn et al., 2015b). In the device, the piezoelectric film straps with the metal electrodes deposited on both sides are woven on a mesh structure of elastic hollow tubes and stitched to each other in a diagonal direction across the mesh structure. The stretchability is attributed to the wavy shapes formed at all crossing points of the tubes and the piezoelectric straps themselves. This textile-based device can either transform mechanical energy from stretching into electrical energy or serve as a tactile sensor to detect vertical force. When used as the energy harvester, the parts of the piezoelectric layer at both of the con-

vex regions over the hollow tubes and concave regions under the hollow tubes undergo compressive stress upon releasing. The compressive stress decreases with the decreasing curvature as the device is stretched by the lateral tensile force. The stretching-releasing cycles cause the variation of strain on the piezoelectric layer, resulting in charge generation in both electrodes. On the other hand, the device can also be used as a capacitive tactile sensor to monitor the magnitude and position of the tactile force. The capacitance is formed between the two separated metal electrodes deposited on the bottom surface of the row piezoelectric strap and the top surface of the column piezoelectric strap. As the vertical force applied on the surface compresses the elastic tubes, the decreased distance between the two electrodes increases the capacitance. Since the capacitance increases with the increasing vertical force, its magnitude informs the magnitude of the force. Furthermore, the sequential measurements of capacitance from multiple row and column straps can help determine the touch position. Consisted of five by five piezoelectric straps, the fabricated device that is capable of adapting to complex deformations can be attached to clothing to monitor the external contact force without external power supply (Fig. 4F). When the device is stretched by 6.7%, the maximum output voltage reaches 51 V at a frequency of 6 Hz, and the maximum power output is 850 μW for a load resistance of 1 MΩ.

In order to harvest the mechanical energy of elbow movements, one wearable fiber-based PEH on an elbow pad is presented. The device is constructed by weaving piezoelectric fiber (hybrid fiber combines $BaTiO_3$ NWs for enhanced piezoelectricity with polyvinyl chloride polymer for flexible properties), cotton threads, and Cu wires together via hand knitting (Fig. 4G). The hybrid fibers and Cu wires woven in the warp and weft directions serve as piezoelectric elements and electrodes, respectively. The cotton threads act as insulating spacers between electrodes to avoid shorting. The piezoelectric fiber of the device in tension from stretching or bending enhances the dipole component to generate positive and negative piezopotentials in the adjacent electrodes, thereby inducing a current in an external load. The device attached to the human arm can generate an output voltage of 1.9 V, current of 24 nA, and power of 10.02 nW for an external load of 80 MΩ from elbow movements (Zhang et al., 2015b).

In summary, various stretchable structures have been successfully applied to fabricate stretchable piezoelectric sensors and energy harvesters. The stretchable structures have endowed superior stretchable properties to these materials, while their excellent piezoelectric properties are preserved. The stretchable and piezoelectric properties of various stretchable piezoelectric devices based on different stretchable structures are summarized in Table 2.

5. Stretchable electrodes for piezoelectric devices

Stretchable electrodes are critical and indispensable components of stretchable piezoelectric energy harvesters and self-powered sensors for practical applications. Apart from high electrical conductivity and excellent stretchability, small resistance changes under considerable tensile strain and stretching cycles represents another desirable features. Highly stretchable electrodes realized by stretchable materials, structural designs or a combination of the two have been summarized in many recent reviews (An and Cheng, 2018; Chen, 2017; Cheng et al., 2015; Choi et al., 2019; Huang et al., 2019; Jung et al., 2019; Kim et al. 2015a, 2019b; Lee et al. 2016b, 2020; Noh, 2016; Wu et al., 2020b; Yu et al., 2017b; Zhao et al., 2017). Therefore, only a few of the highlights will be briefly discussed in this section, with a focus on 1) intrinsically conductive networks and 2) structural design to improve the stretchability (Ahn et al., 2015a). The intrinsically stretchable electrode materials include conductive polymers (Bandodkar et al., 2015; Lee et al., 2016c), soft ionic-hydrogels (Larson et al., 2016), liquid metals (Kim et al., 2015b; Silva et al., 2020), and elastomers with conductive nanocomposite fillers of CNTs (Hong et al., 2017; Xu et al., 2016), metal NWs (Lee et al., 2016a; Tybrandt et al., 2018), and NPs (Lim et al., 2018; Yoon and Kim, 2020). For conventional rigid and brittle conductive materials, extensive ingenious stretchable structures have been proposed and applied to improve their stretchability. Commonly used structures include bucked geometries (Chen et al., 2018a; Weng et al., 2015), serpentine layouts (Dong et al., 2019b), helical/coiled structures (Chu et al., 2018; Son et al., 2019), kirigami designs (Ahn et al., 2015a; Shyu et al., 2015), woven textiles (Liu et al., 2020a; Zang et al., 2015), 3D porous sponge networks (Liang et al., 2020; Liu et al., 2016). The advantages, limitations, and perspectives for further developments of stretchable electrodes with different strategies are also well discussed. Representative latest efforts are focused on performance improvements, such as conductivity (Li et al., 2020c), fatigue durability (Won et al., 2020), and biocompatibility (Fan et al., 2020) under large mechanical deformations.

6. Processing and manufacturing techniques for stretchable piezoelectric materials and devices

Processing techniques for preparing stretchable materials and structures are the foundation for the fabrication of stretchable electronic devices. As summarized in the latest review articles, key processing technologies for stretchable materials include materials synthesis, assembly, and patterning (Kim et al., 2020b). As for the stretchable structures, the corresponding designs and processing methods (e.g., lithographic processes, transfer printing and assembly approaches, and 3D printing techniques) have also been presented and offered in several review articles (Wu et al., 2020a; Xue et al., 2020). In the following part of this section, we will briefly provide an overview of the processing and manufacturing techniques of novel stretchable piezoelectric materials and devices: 1) blending, 2) electrospinning, and 3) deposition. Blending is a simple yet effective method to prepare stretchable piezoelectric composites by dispersing low-dimensional (0D and 1D) materials with high piezoelectric coefficients (e.g. PZT) in a polymer matrix (Jeong et al., 2015; Zhang et al., 2018a). This technology integrates the excellent piezoelectricity of piezoceramics with the mechanical stretchability of polymers, resulting in stretchable piezoelectric composites. The working principle, methods, and applications of electrospinning can be found in the extensive reviews (Alhasssan et al., 2018; Azimi et al., 2020; Xin et al., 2018; Zaarour et al., 2020). In brief, electrospinning is the most commonly used method for fabricating ultrathin piezoelectric fibers (e.g., PVDF fibers) with diameters in the range of a few hundred nanometers (Liu et al., 2019b; Zaarour et al., 2019). Electrospun piezoelectric fibers with different surface morphologies (e.g., porous fibers, wrinkled fibers, and grooved fibers) can be obtained to enhance the stretchability. On the other hand, electrospinning can increase the amount of β phase in the fibers, thereby improving their piezoelectric performance. Various deposition techniques have also been explored, including thermal evaporation, sputtering, pulse laser deposition, and others. After deposition of 2D piezoelectric materials such as PZT or ZnO thin film on a pre-strained elastomeric substrate, the release of the pre-strain leads to the formation of the wavy piezoelectric thin films to offer them flexible and stretchable properties (Kumar et al., 2015; Voiculescu et al., 2019). Additionally, several representative manufacturing techniques (e.g., micro-/nano-fabrication processes and grow-pattern-transfer processes) have been extensively reviewed for the fabrication of stretchable PEHs and self-powered sensors (Kim et al., 2020b; Liu et al., 2018a).

Table 2
Performance comparison of stretchable PEHs based on stretchable structures.

Stretchable structures	Piezoelectric materials	Form	Substrate	Electrodes	Stretchability	Excitation	Output voltage	Output current	Output power	Reference
Out-plane buckled structure	PZT	Ribbons	PDMS	Ag	8%	8% (SS),~0.7 Hz	/	2.5 μA/mm ^{2}	/	Qi et al. (2011)
In-surface buckled structure	PVDF	120 Fibers	PDMS PET	Cu	30%	30% (TS) 0.5 Hz	40 mv	1.2 nA	/	Ding et al. (2015)
Serpentine structure	PVDF	Ribbons	PU	Cu	27.5%	27.5% (TS) 2 Hz	19.8 V (Peak to Peak)	75 nA	/	Yan et al. (2019a)
Fractal serpentine	PVDF	Fibers	PDMS, Ecoflex	LM	200%	200% (TS) 4 Hz	/	150 nA	/	Duan et al. (2017)
Self-similar serpentine	PVDF	Fibers	PDMS, Ecoflex	LM	~300%	120% (TS)	/	20 nA	/	Huang et al. (2017)
Kirigami structure	PVDF	Thin film	PET	Metal	10%	10% (TS) 10 Hz	1.63 V	/	/	Sun et al. (2018)
Kirigami structure	PVDF	Thin film	Kapton	Metal	33%	33% (TS)	333 mv	/	/	Hu et al. (2018a)
Kirigami structure	PVDF	Thin film	PDMS, PET	Metal	30%	30% (TS) 3 Hz	14 V	0.48 μA	/	Sun et al. (2019)
T-joint kirigami structure	BTO, P(VDF-TrFE)	Thin film	ITO glass	Ag	300%	60 N (CF) 5 Hz	6 V	2 μA/cm ^{2}	/	Zhou et al. (2020a)
Helical structure	PVDF	Strap	Elastic core	Ni/Cu alloy	58%	50% (TS) 1 Hz	75 V	/	0.42 mW/cm ^{3}	Kim and Yun (2017)
Woven textiles	PVDF	Strap	Polymer, Elastic tubes	Ni/Cu alloy	6.7%	6.7% (TS) 6 Hz	51 V	28.5 μA	105 mW/m ^{2}	Ahn et al. (2015b)
Woven textiles	PVDF	Strap	PET	Ni/Cu alloy	23%	23% (TS) 6 Hz	/	/	125 μW/cm ^{2}	Song and Yun (2015)
Woven textiles	CNT-PZT composite	Strap	PDMS	Ag NWs	50%	50% (TS) 4 Hz	11.3 V (Peak to Peak)	8.4 μA	48 μW	Kim and Yun (2019)
Triaxial woven textiles	PVDF	Fibers	SR	Ag coated nylon	58%	0.023 MPa Compressive pressure	380 mV	/	0.16 μW	Mokhtari et al. (2019)
						Bending 0.6 Hz	150 mV		4.62 μW	

7. Theoretical modeling of stretchable piezoelectric energy harvesters and sensors

7.1. Mechanics analysis

While analytical solutions are not available for stretchable piezoelectric energy harvesters and sensors that are under complicated mechanical deformations, the analysis of the coupled mechanical and electrical behavior of the device upon simple bending can still provide critical insights into the experimental results. The configuration of a buckled device includes PZT ribbons on top of a soft substrate (Fig. 5AB) (Dagdeviren et al., 2014). The coordinate x_1 is defined along the longitudinal direction, x_2 is along the width direction (into the diagram), and x_3 is along the thickness direction (also the piezoelectric polarization direction). The substrate has an undeformed length of L and a compression of ΔL. The out-of-plane displacement w of the buckled device takes the form

$$w = \frac{A}{2}\left(1 + \cos\frac{2\pi x_1}{L}\right) \tag{1}$$

Neglecting the strain energy and the electric potential energy of the PZT ribbon along with the shear stress between the ribbons and substrate, the amplitude A has been obtained by using the method of minimization of total energy as (Chen et al., 2015b; Song et al., 2009)

$$A \approx \frac{2}{\pi}\sqrt{L\cdot\Delta L - \frac{\pi^2 t_{PI}^2}{3}} \tag{2}$$

For thin-film structures, the second term inside the square root can be neglected, and the amplitude can be approximated as

$$A \approx \frac{2}{\pi}\sqrt{L\cdot\Delta L} \tag{3}$$

The axial (bending) strain at the center of PZT ribbons is given as

$$\varepsilon_m = w''h \approx -4\pi\frac{(EI)_{PI}}{(EI)_{comp}}\frac{h}{L}\sqrt{\frac{\Delta L}{L}} \tag{4}$$

where the bending stiffnesses EI of the PI substrate and composite segment of the device are given as

$$(EI)_{PI} = \frac{E_{PI} t_{PI}^3}{12} \tag{5-a}$$

respectively, and E_i and t_i are Young's modulus and thickness of the i-th layer, respectively. The distance (h) between the center of PZT and the neutral axis can be located through bending analysis as

$$y_{neutral} = \frac{\sum_{i=1}^{n} E_i t_i \left[2\left(\sum_{j=1}^{i} t_j - t_i\right)\right]}{2\sum_{i=1}^{n} E_i t_i} \tag{6}$$

7.2. Piezoelectric and circuit analysis

The coupled mechanical and electrical behavior of a piezoelectric material can be modeled by the following constitutive equations in tensor form:

$$T_{ij} = c_{ijkl}^{E} S_{kl} - e_{kij} E_k \tag{7-a}$$

$$D_i = e_{ikl} S_{kl} + k_{ij}^{s} E_k \tag{7-b}$$

where T is the mechanical stress, S is the mechanical strain, E is the electrical field, and D is the electric displacement. The constants c_{ijkl}^{E}, e_{kij} and k_{ij}^{s} are the elastic, piezoelectric, and dielectric constants, respectively. The superscript "E" denotes a constant electrical field (e.g., short-circuit), and "S" denotes a constant strain (e.g., clamped). The first equation describes the *converse piezoelectric effect*, i.e., a mechanical strain or displacement is produced when an electric field is applied to the piezoelectric material. This effect has been utilized for actuation applications. The second equation describes the *direct piezoelectric effect*, i.e., an electric charge is produced when a mechanical strain is applied to the material. This is the effect that has been utilized for sensing and energy harvesting applications. The two constitutive equations can be explicitly expressed in a matrix form for orthotropic piezoelectric materials:

$$\begin{bmatrix} \sigma_{11} \\ \sigma_{22} \\ \sigma_{33} \\ \sigma_{23} \\ \sigma_{31} \\ \sigma_{12} \end{bmatrix} = \begin{bmatrix} c_{11} & c_{12} & c_{13} & 0 & 0 & 0 \\ c_{12} & c_{22} & c_{13} & 0 & 0 & 0 \\ c_{13} & c_{13} & c_{33} & 0 & 0 & 0 \\ 0 & 0 & 0 & c_{44} & 0 & 0 \\ 0 & 0 & 0 & 0 & c_{55} & 0 \\ 0 & 0 & 0 & 0 & 0 & c_{66} \end{bmatrix} \begin{bmatrix} \varepsilon_{11} \\ \varepsilon_{22} \\ \varepsilon_{33} \\ 2\varepsilon_{23} \\ 2\varepsilon_{31} \\ 2\varepsilon_{12} \end{bmatrix} - \begin{bmatrix} 0 & 0 & e_{31} \\ 0 & 0 & e_{32} \\ 0 & 0 & e_{33} \\ 0 & e_{24} & 0 \\ e_{15} & 0 & 0 \\ 0 & 0 & 0 \end{bmatrix} \begin{bmatrix} E_1 \\ E_2 \\ E_3 \end{bmatrix} \tag{8-a}$$

$$\begin{bmatrix} D_1 \\ D_2 \\ D_3 \end{bmatrix} = \begin{bmatrix} 0 & 0 & 0 & 0 & e_{15} & 0 \\ 0 & 0 & 0 & e_{24} & 0 & 0 \\ e_{31} & e_{32} & e_{33} & 0 & 0 & 0 \end{bmatrix} \begin{bmatrix} \varepsilon_{11} \\ \varepsilon_{22} \\ \varepsilon_{33} \\ 2\varepsilon_{23} \\ 2\varepsilon_{31} \\ 2\varepsilon_{12} \end{bmatrix} - \begin{bmatrix} k_{11} & 0 & 0 \\ 0 & k_{22} & 0 \\ 0 & 0 & k_{33} \end{bmatrix} \begin{bmatrix} E_1 \\ E_2 \\ E_3 \end{bmatrix} \tag{8-b}$$

where σ and ε represent mechanical stress and strain, respectively, and k is the dielectric constant at a constant strain. Many piezoelectric materials can be treated as transversely isotropic, for instance, PZT ceramics. In this case, some of the elastic, piezoelectric, and dielectric constants are dependent on the others as

$$\begin{aligned} c_{22} &= c_{11}, c_{23} \\ &= c_{13}\ , c_{55} \\ &= c_{44}, c_{66} \\ &= \frac{c_{11} - c_{12}}{2}, e_{24} \\ &= e_{15}, e_{32} \\ &= e_{31}, k_{22} \\ &= k_{11} \end{aligned} \tag{9}$$

Given the plan-strain condition $\varepsilon_{22} = 0$ and plane stress condition $\sigma_{33} = 0$ for the PZT ribbons, manipulation of the constitutive equations, Eqs. (8-a) and (8-b), yields the electric displacement (Dagdeviren et al., 2014)

$$D_3 = \bar{e}\varepsilon_{11} + \bar{k}E_3 \tag{10}$$

where the effective piezoelectric constant and effective dielectric constant are defined as

$$\bar{e} = e_{31} - \frac{c_{13}}{c_{33}} e_{33} \tag{11-a}$$

$$\bar{k} = k_{33} + \frac{e_{33}^2}{c_{33}} \tag{11-b}$$

As N groups of PZT ribbons connected in series generate an overall output voltage of V (Dagdeviren et al., 2014), the voltage between the top and bottom of each PZT ribbon is V/N. Assuming a uniform electric field in the PZT ribbon and taking the normal stress at the center of the ribbon layer, the electric displacement expression (10) can be written as

$$D_3 = \bar{e}\varepsilon_m + \frac{\bar{k}V}{Nt_{PZT}} \tag{12}$$

In each PZT ribbon group, the electric current as a result of the produced electric displacement is:

$$i = -A_{PZT}\dot{D}_3 = -A_{PZT}\bar{e}\dot{\varepsilon}_m - A_{PZT}\frac{\bar{k}\dot{V}}{Nt_{PZT}} \tag{13}$$

where A_{PZT} is the total surface area of each ribbon group. When the device is connected to an external resistive load R, the voltage across the load is V, and the current is the same as that in those ribbon groups in series, i.e., $V/R = i$, which leads to the first-order differential equation for the output voltage:

$$\frac{A_{PZT}\bar{k}}{Nt_{PZT}}\dot{V} + \frac{1}{R}V = -A_{PZT}\bar{e}\dot{\varepsilon}_m \tag{14}$$

This is the governing equation that can be used to analytically determine the output voltage V given the PZT strain in Eq. (4) for a given compression ΔL. For zero initial condition, i.e., $V(t = 0) = 0$, the voltage can be determined for an arbitrary PZT strain function ε_m as (Dagdeviren et al., 2014):

$$V(t) = \frac{-\bar{e}Nt_{PZT}}{\bar{k}} e^{\frac{Nt_{PZT}}{A_{PZT}R\bar{k}}t} \int_0^t \frac{d\varepsilon_m}{dt} e^{\frac{Nt_{PZT}}{A_{PZT}R\bar{k}}t} dt \tag{15}$$

7.3. System behaviors

The measured output voltage of the piezoelectric device indicates 1) the output voltage can change between positive and negative even though the strain in the piezoelectric material is always positive during the applied cycling load; 2) the voltage measurement strongly depends on the resistance of the voltmeter (Fig. 5C) (Su et al., 2015a). To investigate these system behaviors, assuming the strain expression

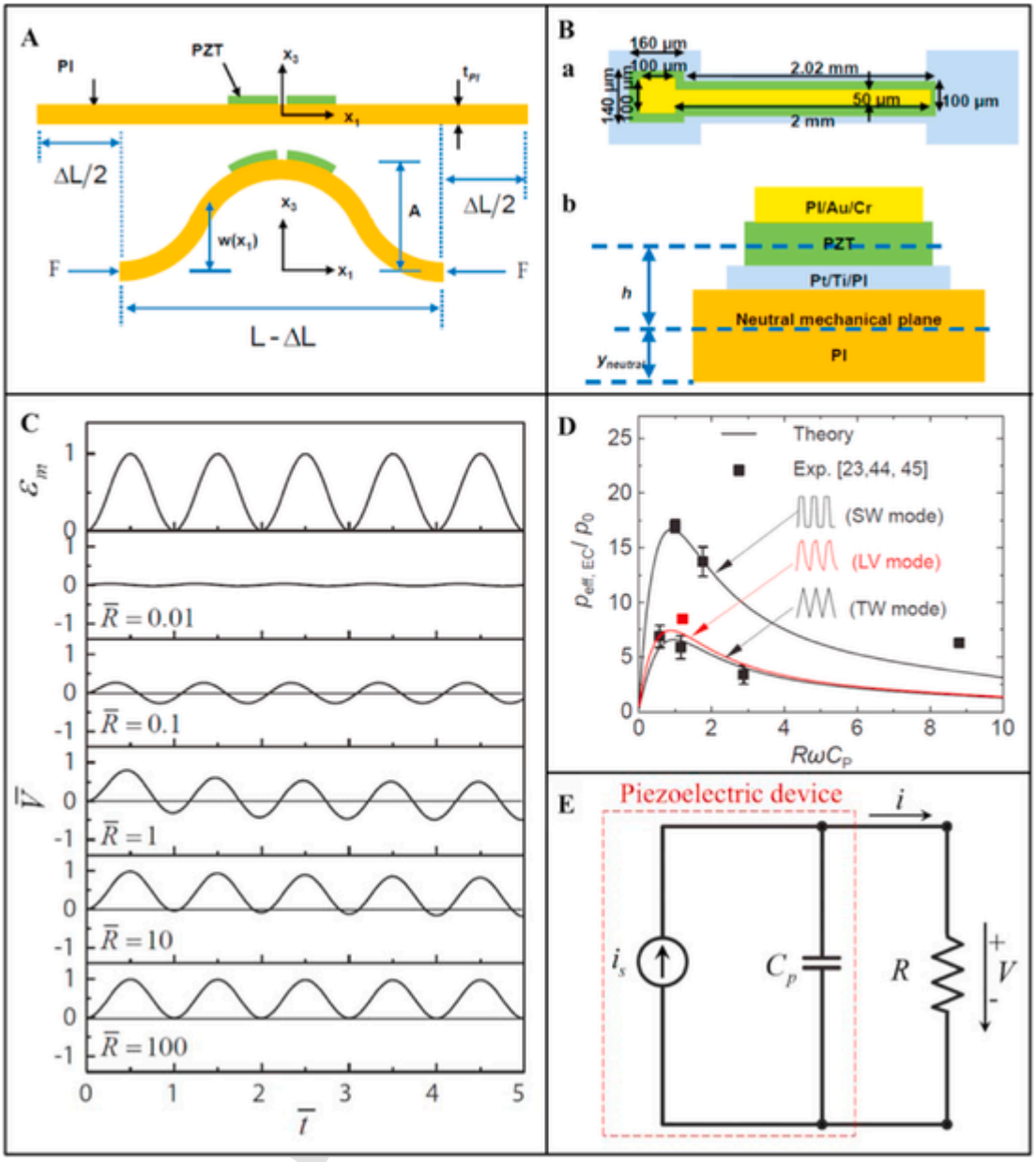

Fig. 5. Schematic of theoretical models and their electromechanical results. (**A**) Schematic illustrations of theoretical buckling shape for a stretchable PEH under compression. (**B**) (a) Top view of a single PZT ribbon structure. (b) Cross-sectional view showing the neutral mechanical plane of the designed device. Reproduced with permission from (Dagdeviren et al., 2014); Copyright 2014, National Academy of Sciences. (**C**) Influence curves of the dimensionless resistance on the dimensionless output voltage. Reproduced with permission from (Su et al., 2015a); Copyright 2015, WILEY-VCH Verlag GmbH & Co., KGaA, Weinheim. (**D**) The normalized effective power density of the energy conversion circuit $P_{\text{eff, EC}}/P_0$ versus $R\omega C_p$ for TW, LV, and SW modes. Reproduced with permission from (Lü et al., 2019); Copyright 2019, Elsevier Ltd. (**E**) Equivalent circuit of the piezoelectric device connected to a resistive load.

$$(EI)_{comp} = \sum_{i=1}^{n} E_i t_i \left[\frac{t_i^2}{3} + \left(\sum_{j=1}^{i} t_j - y_{neutral} \right) \left(\sum_{j=1}^{i} t_j - y_{neutral} - t_i \right) \right] \tag{5-b}$$

$\varepsilon_m = \left[1 - \cos(2\pi\bar{t})\right]/2$ solves for the voltage from Eq. (14) in a dimensionless form as:

$$\bar{V} = \frac{\pi\bar{R}}{\sqrt{1+4\pi^2\bar{R}^2}} \sin\left[2\pi\bar{t} - \arctan(2\pi\bar{R})\right] + \frac{2\pi^2\bar{R}^2}{1+4\pi^2\bar{R}^2} e^{-\bar{t}/\bar{R}} \tag{16}$$

where the dimensionless voltage, time, and resistance are defined as

$$\bar{V} = \frac{\bar{k}V}{-\bar{e}Nt_{PZT}}, \bar{t} = \frac{t}{T}, \bar{R} = \frac{A_{PZT}\bar{k}R}{Nt_{PZT}T} \tag{17}$$

and T is the period of the cycling load. The sign of the first term on the right-hand side of Eq. (16) changes between positive and negative.

The second term decreases quickly if the dimensionless resistance $\bar{R}$ is small. As $\bar{R}$ increases, the dimensionless voltage moves into the positive range gradually and becomes nonnegative completely when $\bar{R}$ is infinitely large, i.e., open circuit.

The influences of excitation frequency, excitation amplitude, load resistance, and excitation modes, including triangle wave (TW) mode (Chen et al., 2015b), square/rectangular wave (SW) mode (Su et al., 2015a) and left ventricle (LV) mode (Dagdeviren et al., 2014; Lu et al., 2015), have been analytically and experimentally studied (Chen et al., 2015b; Dagdeviren et al., 2014; Lu et al., 2015; Su et al., 2015a). Fig. 5D presents a comparison study of the three excitation modes and the power density results (Lü et al., 2019). The normalized power density under quasi-SW mode is found to be much larger than that under TW and LV modes. Additionally, there exists an optimal value of parameter $R\omega C_p$, i.e., close to one, for maximized power density.

7.4. Comments and perspective on modeling and system behavior

In addition to the discussions in the original papers, this review paper would like to add discussions from a system dynamics perspective, to help further understand the system behavior. Equation (14) is the governing differential equation that relates the strain in PZT to the output voltage. It is important to note that the forcing function on the right-hand side of the equation is related to the derivative of the strain ε_m, not the stress directly. In other words, the change of the strain is the true forcing function that drives the system dynamics. Though the strain is always nonnegative, the rate of change of strain switches between positive and negative. Moreover, the forced response of the system, i.e., output voltage, consists of a transient (or natural response) component and a steady-state (or forced) component, which are clearly shown in Eq. (16). The first term on the right-hand side of the equation is the sinusoidal steady-state response component (centered about zero) due to the sinusoidal excitation, while the second term on the right is the transient component that decays with time. The speed of decay or charge leakage through the resistance is represented by the time constant of the system, which can be found to be $A_{PZT}\bar{k}R/\left(Nt_{PZT}\right)$.from Eq. (16). Therefore, as the load resistance increases, the time constant increases, and it takes longer for the positive transient component to die out. These explain the observations in Fig. 5C (Su et al., 2015a), where the contribution of the transient component is significant during the first few cycles of the response when the load resistance is large, effectively adding a positive offset in the overall response. Besides, the SW excitation mode leads to a higher power density compared to the TW and LV modes (Lü et al., 2019). This can be explained by the much larger rate of change in strain in PZT as a result of rapid loading to maximum stress for the SW excitation mode.

The influence of excitation frequency and load resistance can be conveniently studied by using the equivalent circuits of the system, as shown in Fig. 5E. The circuit is obtained from Eq. (14) by noting the right-hand side of the equation is equivalent to the source current i_s, and the first term on the left-hand side is the current in the internal capacitor C_p and the second term is the current in the resistor R with the quantities defined as:

$$i_s = -A_{PZT}\bar{e}\dot{\varepsilon}_m, C_p = \frac{A_{PZT}\bar{k}}{Nt_{PZT}} \tag{18}$$

The current source and the internal capacitor as a whole (dashed box in Fig. 5E) represent the piezoelectric device. In fact, it is a common representation of piezoelectric transducers neglecting the internal leakage resistance (Kim et al., 2004; Kon and Horowitz, 2008). This is not surprising because both sensing and energy harvesting applications are based on the same piezoelectric effect, i.e., the direct effect.

Frequency-domain analysis can be applied to this equivalent circuit to obtain the voltage across the load resistance R for harmonic responses:

$$V = \frac{RI_s}{\sqrt{1+\left(\omega C_p R\right)^2}} \tag{19}$$

where I_s represents the amplitude of the equivalent source current. It can be seen that the output voltage increases monotonously with the load resistance, reaching its maximum at the open circuit (graphically shown Fig. 5C). The AC power dissipated in R can be obtained as:

$$P = \frac{RI_s^2}{1+\left(\omega C_p R\right)^2} \tag{20}$$

which initially increases as R increases, reaches a maximum value, and then decreases. It can be shown that the optimal condition at the maximum is:

$$\omega C_p R = 1, R = 1/\left(\omega C_p\right) \tag{21}$$

which agrees with Lü et al.'s results shown in Fig. 5D. From a circuit perspective, a large portion of the source current flows into the load resistance branch when the resistance is very low. However, power is still low because the resistance is too low. When the resistance is very large, only a small portion of the source current flows into the load resistance branch, resulting in a low power as well. There exists an optimal balance between the magnitude of the resistance and the amount of current following into the resistor, which occurs when the condition given in Eq. (21) is satisfied. The concept of matching the electrical load to system parameters for optimal power, i.e., impedance matching, has been extensively discussed for piezoelectric energy harvesting (Kim et al., 2007; Kong et al., 2010; Liao and Liang, 2018).

As a final note, the discussed analytical model is based on a static analysis of a buckled membrane. Also, it is a piezoelectric model that only considers the direct piezoelectric effect, not the converse piezoelectric effect. In other words, it neglects the backward coupling from the electrical domain into the mechanical domain that also changes the structural dynamics of the system. In contrast, a fully coupled model for piezoelectric systems (Hagood et al., 1990) has been extensively used in vibration-based piezoelectric energy harvesting analysis (Liao and Sodano, 2008; Shu and Lien, 2006). The backward coupling could have a significant influence on the system response of a vibration energy harvester due to the electrically induced damping (Lesieutre et al., 2004; Liang and Liao, 2009; Liao and Sodano, 2009). Vibration energy harvesters are usually designed to operate near their natural frequency to utilize the large structural response due to resonance. The effect of damping and backward coupling is substantial. However, stretchable energy harvesting devices for wearable and biomedical applications are generally subjected to very low-frequency excitations, and operate far away from the resonance. Therefore, it is reasonably accurate to use a static structural model for mechanical analysis and a piezoelectric transducer model for electromechanical analysis.

8. Applications of stretchable piezoelectric devices in biomedicine

While the flexible and stretchable diagnostic and surgical devices integrated on the human body could provide advanced health monitoring and therapeutic capabilities, their continuous operation is limited by the need to replace the battery. As a power source, flexible and stretchable energy harvesters that can provide sustained and sufficient electric energy for various medical devices eliminate the necessity of battery replacement. The resulting system is of great significance for real-time monitoring, diagnosis, and continuous therapy. In this section, we will introduce the latest developments of the flexible

and stretchable PEHs in wearable and implantable electronic devices. Power management and biocompatibility are also discussed.

8.1. Applications in wearable biomedical devices

Wearable medical devices enable non-invasive monitoring of human physiological or pathological signals, including breathing (Güder et al., 2016), arterial pulse (Park et al., 2017), body temperature (Chen et al., 2015a; Han et al., 2018), heart rate (Lee et al., 2018a; Li et al., 2017), blood glucose (Chen et al., 2017b), blood pressure (Ma et al., 2018), and blood oxygen (Li et al., 2017). The integration of wearable piezoelectric generators with these devices has promoted the development of self-powered medical devices. In addition to harvesting biomechanical energy from human motion for powering wearable devices, flexible and stretchable PEHs can also be used as piezoelectric self-powered sensors for health monitoring in biomedicine.

Based on a sandwich structure, a high-performance bulk form PIMNT/epoxy 2-2 composite flake is integrated with interdigital electrodes (IDEs) film and a PET cover. The resulting flexible PEH can generate an open-circuit of 54.2 V, extrapolation current of 6.7 μA, and instantaneous power as high as 105 μW while withstanding a small bending radius of 2.2 cm (Fig. 6A) (Zeng et al., 2017). Placing this flexible device on the back of the knees allows it to harvest biomechanical energy from walking or running. The output voltage can reach 10–15 V under a slow walking at a frequency of 1.3 Hz or 20–25 V during a relatively fast running at a frequency of 2.2 Hz. The generated output power is sufficient for the power requirement of 12 red LEDs. An integrated wearable piezoelectric-driven supercapacitor based on PVDF nanofibers can efficiently harvest the mechanical energy induced by human motion and store the induced electric energy to provide sustainable energy supply for wearable electronics (Fig. 6B) (He et al., 2019). Based on electrospun nanocomposite fiber mats comprising PVDF, graphene nanosheet, and barium titanate, the fabricated PEHs with high piezoelectricity and good flexibility can efficiently harvest energy from human activities (e.g., wrist bending, finger tapping, and foot stepping) (Fig. 6C) (Shi et al., 2018b). The device can yield an output power of 4.1 μW for a bending deformation caused by a compressive displacement of 4 mm at a frequency of 2 Hz. The output voltage can reach 7.7 V upon wrist bending, whereas it becomes 7.8 V and 2.8 V under stepping, with the flexible PEH placed under the foot heel and toe, respectively. These results demonstrate the potential of fabricated devices to harvest the biomechanical energy for powering wearable electronics.

Piezoelectric sensors have also made great achievements in health monitoring. Growing ZnO NWs arrays on ultra-thin Al-foil enables supersensitive sensors to detect small physical motions without any external power supply. Attaching a sensor with a size of 5 mm × 13 mm to the skin near a human eye readily detects the wrinkle of the face induced by closing and opening of the eye (Fig. 6D-ab) (Lee et al., 2013). The device can also efficiently harvest energy from very slight human motion due to its high flexibility. The maximum output volt-

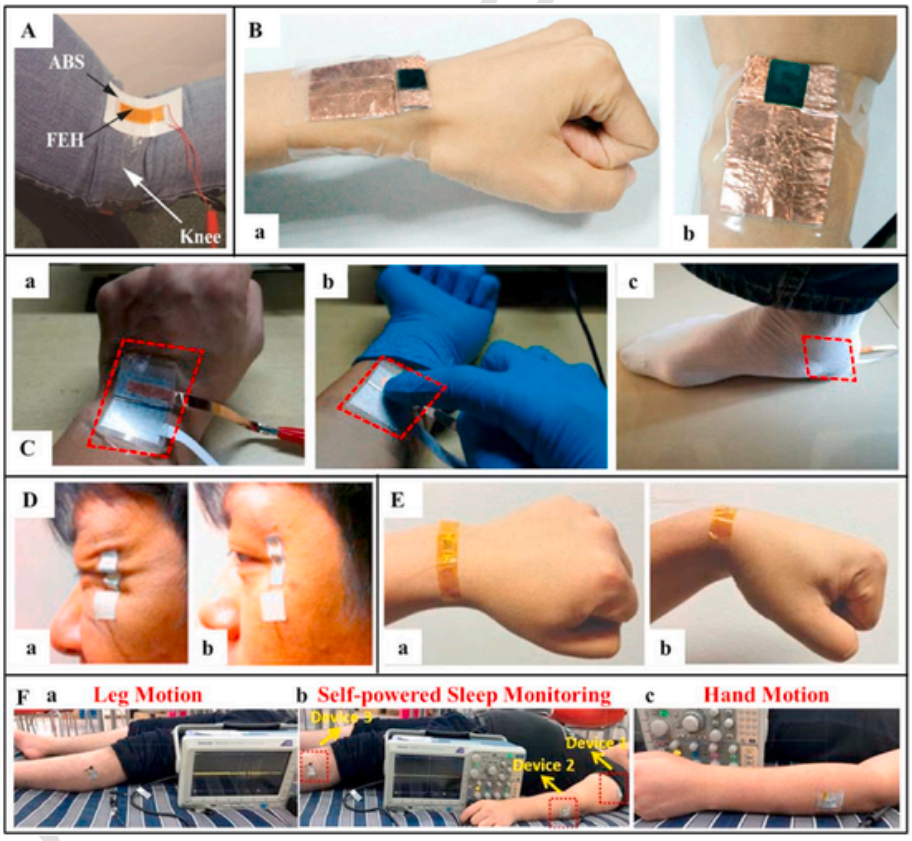

Fig. 6. Flexible and stretchable PEHs as wearable devices. (**A**) A flexible energy harvester placed on the back of the knees for harvesting energy from bending deformation. Reproduced with permission from (Zeng et al., 2017); Copyright 2017, Elsevier Ltd. (**B**) The self-powered system consists of the PEH based on PVDF nanofibers and a supercapacitor attached (a) on the wrist and (b) its top view. Reproduced with permission from (He et al., 2019); Copyright 2018, American Chemical Society. (**C**) Optical images of the stretchable PEHs for harvesting mechanical energies from (a) wrist bending, (b) finger taping, and (c) foot stepping by the heel. Reproduced with permission from (Shi et al., 2018b); Copyright 2018, Elsevier Ltd. (**D**) An ultra-flexible PEH attached to the skin near the human eye to detect the wrinkling of a human face during blinking. Reproduced with permission from (Lee et al., 2013); Copyright 2013, WILEY-VCH Verlag GmbH & Co., KGaA, Weinheim. (**E**) A PMN-PT-based piezoelectric sensor attached to the human wrist for measuring wrist movement. Reproduced with permission from (Chen et al., 2017c); Copyright 2017 John Wiley and Sons. (**F**) Self-powered health monitoring system with the energy harvested from human motion to monitor (a) leg motion and (c) hand motion during sleep, with a schematic shown in (b). Reproduced with permission from (Vivekananthan et al., 2019); Copyright 2019, Elsevier Ltd.

age and current can reach ca. 0.2 V and 2 nA during the blinking motion. Attaching the ultra-thin flexible PEH with a size of 3 mm × 10 mm to a right eyelid on the center also detects the movement of the eyeball from side to side (Lee et al., 2014). The PEH is strained when the eyeball passes under the device, and then released after the eyeball moves to the side. The recorded output voltages and currents under the slow (~0.4 Hz) and rapid motion (~1.6 Hz) can provide valuable information for the sleep patterns, tiredness, and brain activities. Exploiting the excellent piezoelectric and pyroelectric properties of single-crystal PMN-PT ribbons yields a flexible acoustic sensor suitable for monitoring and energy harvesting (Chen et al., 2017c). The application of the resulting sensors to detect motions ranges from the large-scale bending movements of the human wrist (Fig. 6E) to the subtle motions of the face and neck during speaking or coughing. Impregnating lead-free (1-x) $KNaNbO_3$-x $BaTiO_3$ (KNN-x BTO) NPs into the PDMS matrix yields a composite film as flexible piezoelectric composite nanogenerators (PCNGs). It is found from experiments that the PCNGs of KNN-0.02 BTO show the maximum electrical output; the maximum output voltage, current, and power density for a 10 MΩ load can reach 58 V, 450 nA, and 3.25 mW/m^2, respectively (Vivekananthan et al., 2019). Attaching the designed PCNGs to the legs and hands of the human body also allows their use as an active self-powered sensor to monitor physical activities during sleep (Fig. 6F). The real-time electrical response can be used for the diagnosis of sleeping disorders and other neurological disorders. It is worth noting that there are minimal hazardous concerns to humans because the KNN is lead-free.

8.2. Applications in implanted biomedical devices

Compared to wearable devices, the power supply in implantable devices is more critical as battery replacement is more difficult for implanted devices inside the human body. Because ZnO is biocompatiable, ZnO NW based PEHs have great potential as implanted devices to harvest biomechanical energy from the motions of heartbeat and other internal organs (Li et al., 2010). The average output power from these devices attached to the heart of a living rat reaches up to 90 nW. Although only a relatively small output power is obtained, the result still presents a viable power supply for self-powered implantable biomedical electronics. Improved piezoelectric performance with PZT thin film is demonstrated through stretching and bending experiments (Qi et al., 2011). A biocompatible flexible PEH based on PZT ribbons for powering the implantable devices can yield significant electrical power by harvesting biomechanical energy from motions of the heart, lung, and diaphragm (Dagdeviren et al., 2014). *In vivo* tests performed in bovine and ovine with devices attached to different regions of the heart (right ventricle (RV), left ventricle (LV) base and free wall of the heart) (Fig. 7A–a) and lung (Fig. 7A-bc) have simulated the scenario of application in the human body. The anchoring scheme with sutures at three points is applied to fix the device onto the epicardium with focal contact to avoid constraint on cardiac motion, during which there is no detectable change in cardiac conduction or epicardial motion. Therefore, the implanted PEH is believed to pose a negligible burden on the heart. The maximum output voltage of a harvester with single-layer PZT thin film is higher than 3.7 V, sufficient to maintain the continuous operation of an implanted cardiac pacemaker. Similarly, an ultra-flexible PEH based on PZT thin film can be conformally integrated with a heart for harvesting biomechanical energy from the heart motion (Fig. 7B) (Lu et al., 2015). The device fixed on the epicardium of swine is flattened and bent during the heart relaxation in diastoles (Fig. 7B–a) and contraction in systoles (Fig. 7B–b). The Peak to peak voltage can reach as high as 3 V when the device is fixed on the apical anterior ventricular wall (a region between LV apex and RV). Due to ultra-flexibility and lightweight of the PEH, the normal physiological activities of the swine will not be affected in the experiment, which indicates that the heart does not endure extra burden in the presence of PEH. In the human circulatory system, the function of the heart is to continuously drive blood through arteries into organs and tissues. Approximately 10% diameter change of the carotid artery between the systolic and diastolic period (Bussy et al., 2000; Dammers et al., 2003) provides a possibility to indirectly harvest heartbeat energy from the arterial pulsation, minimizing disturbance to the function and structure of the heart. By wrapping the device around the ascending aorta of a porcine, an implantable PVDF-based PEH can indirectly harvest heartbeat energy *in vivo*, with the maximum output voltage of 1.5 V, current of 300 nA, and instantaneous power of 30 nW for a heart rate of 120 bpm and blood pressure of 160/105 mmHg (Zhang et al., 2015a). Without contact with the blood, the risks of thrombosis and changes in the blood flow can be avoided. Furthermore, the cardiac structure and function are minimally affected by the device wrapped around the ascending aorta.

Self-powered implantable sensing devices are also desirable for providing real-time, accurate, and continuous monitoring of important physiological signals. As an example, real-time monitoring of blood pressure greatly reduces the risk of secondary disease (e.g., arteriosclerosis and cerebrovascular diseases) for patients with hypertension. A flexible PVDF based self-powered implantable blood pressure monitoring system has been presented. The device could harvest biomechanical energy by wrapping it around the ascending aorta (Fig. 7C) (Cheng et al., 2016). The robust self-powered sensing capability is demonstrated from three aspects: (1) high output power of 2.3 μW *in vitro* and 40 nW *in vivo* during the expansion and retraction of the aorta; (2) excellent linearity ($R^2 > 0.971$) between the output voltage and blood pressure in the experiment performed in adult Yorkshire porcine *in vivo*; (3) high sensitivity of 14.3 mV/mmHg *in vivo*; and (4) superior stability of more than 50,000 operating cycles. These good characteristics indicate a great potential of the proposed blood pressure monitoring system for real-time blood pressure monitoring. It is highly desirable to utilize materials with a high piezoelectric coefficient to further increase conversion efficiency. The single crystalline PMN-PT has exceptional piezoelectric charge constant of d_{33} up to 2500 pC/N, which is almost 80 times higher than that of PVDF and 4 times higher than that of PZT. Integrating PMN-PT thin film on rubber substrate successfully yields a highly-efficient stimulator to achieve a self-powered artificial cardiac pacemaker (Fig. 7D) (Hwang et al., 2014). Without any external power supply, the instantaneous electric output from the fabricated devices can directly stimulate a rat heart. The flexible PMN-PT stimulator connected with electrodes electrically stimulates the living heart of an anesthetized rat (Fig. 7D-ab). With sensing terminals attached on the rat legs to monitor its electrocardiogram (ECG), the typical ECG of a normal rat heart before stimulation such as QRS complex, P wave, and T wave is clearly observed (Fig. 7D–c). When the flexible PMN-PT thin film is bent and released periodically, the generated energy of 2.7 μJ (larger than the threshold energy of 1.1 μJ for a normal live rat) from one bending motion triggers the action potential for artificially contracting the heart. The corresponding spike peaks that appear on the natural heartbeat of the rat in the ECG (Fig. 7D–d) demonstrate the flexible PMN-PT stimulator is capable of real-time functional electrical stimulation. The.

demonstrated systems have great potential in normalizing cardiac function and other biomedical applications. As shown in Fig. 7E, the kirigami-based stretchable and self-powered sensing system can simultaneously enhance electrical performance and stretchability. When combined with a wireless communication module, the kirigami-based wireless stretchable piezoelectric strain sensor mounted on different surfaces allows for cardiac monitoring and human body tracking (Sun et al., 2019). A nearly linear relationship between the strain and the output voltage signal is observed from measurements of the surface strain of pig hearts and knee flexion. With the help of a near-field com-

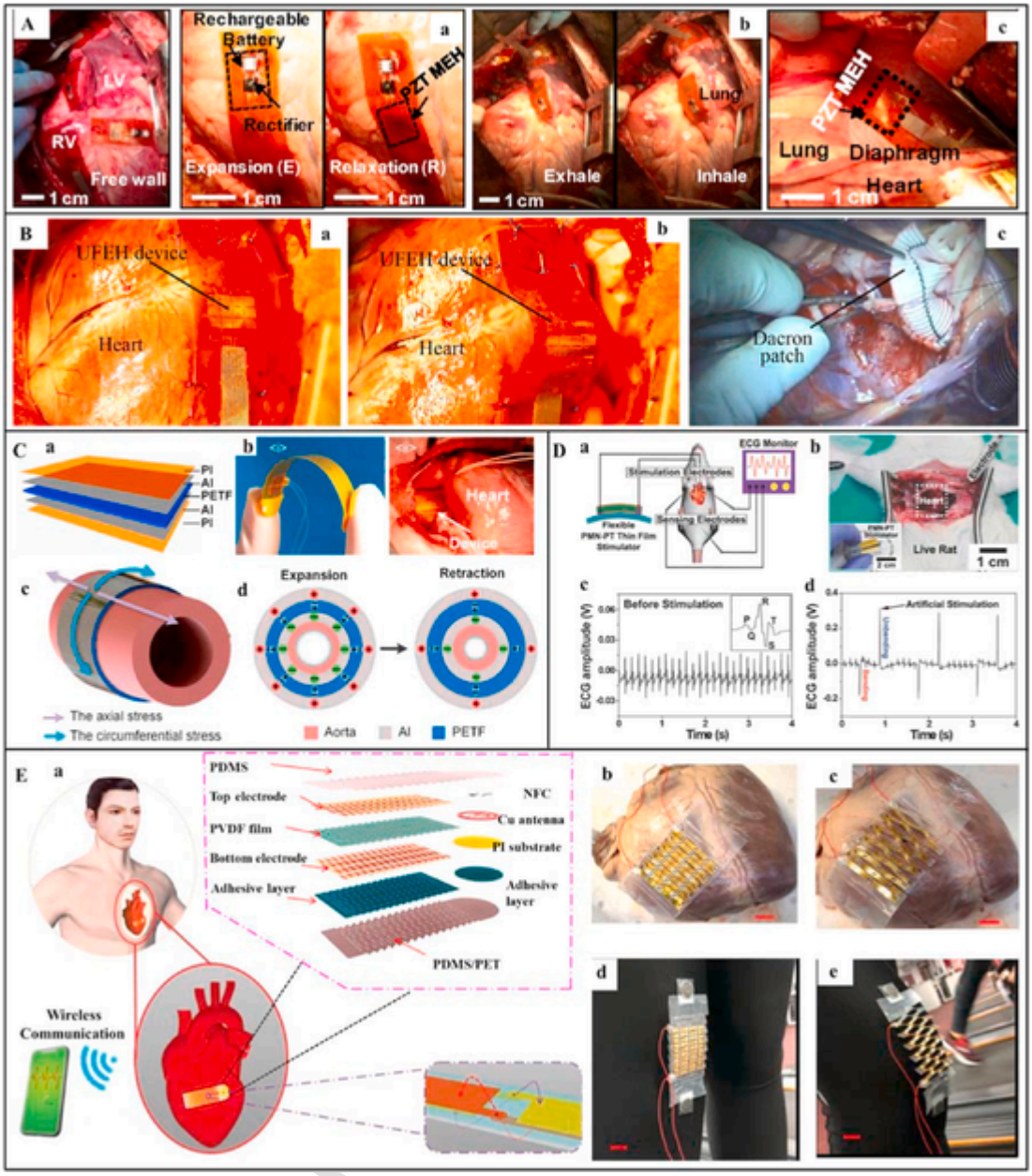

Fig. 7. Applications of flexible and stretchable piezoelectric energy harvester for implanted devices. (A) (a) Photograph of PZT-based PEH attached on RV, LV, and free wall of a bovine heart. (b) Photograph of a PEH mounted on the bovine (a) lung and (b) diaphragm. Reproduced with permission from (Dagdeviren et al., 2014); Copyright 2014, National Academy of Sciences. (**B**) *In vivo* testing: the PEH fixed on the heart is (a) flatted when the heart relaxes in diastoles and (b) bent when the heart contracts in systole. (c) Photograph of the Dacron patch, which is widely used in the cardiovascular operation. Reproduced with permission from (Lu et al., 2015); Copyright 2015, Nature Publishing Group. (**C**) PEH based on a polarized PVDF thin film. (a) Exploded view of the device structure with a multilayer thin film. (b) Photograph of the designed device with high flexibility and the device wrapped around the porcine ascending aorta. (c) The axial, circumferential stress distribution in expanded aorta wall. (d) The induced charge distributions in the device under expansion and retraction state. Reproduced with permission from (Cheng et al., 2016); Copyright 2016, Elsevier Ltd. (**D**) Self-powered cardiac pacemaker based on flexible PMN-PT thin film. (a) A schematic of the experimental setup for artificial cardiac pacemaker powered by a flexible PMN-PT thin-film. (b) Photograph of the animal experiment to stimulate the living heart. The inset shows a photograph of a flexible PMN-PT heart stimulator. (c) The measured ECG of the rodent before the artificial stimulation. The inset presents the typical P wave, T wave, and QRS complex of the heart beating. (d) The remarkable artificial peaks on the ECG made by the periodic motion of bending and unbending of the flexible PEH. Reproduced with permission (Hwang et al., 2014); Copyright 2014, WILEY-VCH Verlag GmbH & Co., KGaA, Weinheim. (**E**) Kirigami-based wireless and self-powered sensing system. (a) A schematic illustration of the designed device with a stretchable sensor and a wireless patch in multilayered structures. *In vitro* and *ex vivo* tests for energy harvesting from heartbeat during (b) contraction and (c) relaxation of a fresh pig heart, and movement of knee joint in the (d) initial and (e) flexion state. Reproduced with permission from (Sun et al., 2019); Copyright 2019, WILEY-VCH Verlag GmbH & Co., KGaA, Weinheim.

munication (NFC) module, the collected signals can be transmitted wirelessly. A series of *ex vivo*, *in vitro*, and on the body tests demonstrate the practical utility of the designed kirigami-based wireless and self-powered sensing systems.

8.3. Power management

Power management circuit (PMC) is one of the key components in a piezoelectric energy harvesting system, which is responsible for controlling both the storage and usage of harvested energy. PMC has two essential functions: 1) converting alternating current (AC) generated

by PEHs to direct current (DC), and 2) matching the impedance of the harvester for maximum power output (Asthana and Khanna, 2020). Effective power management can reduce the consumption of electronic systems, thereby improving efficiency. In general, the electrical outputs come in intermittent or periodic pulses when driven by human activities (e.g., walking/running/talking, or the motions of hearts, lungs, and other organs), which cannot directly power biomedical sensors. Therefore, a capacitor or rechargeable battery as the energy-storage device is needed to store the generated energy. For example, a chip-scale rechargeable battery with a Schottky bridge rectifier mounted on the same flexible substrate with PEHs is used to store the harvested energy (Dagdeviren et al., 2014). At the same time, the energy management circuit is explored to address the impedance mismatch issue for maximized energy extraction (Shi et al., 2018a). Many advanced PMCs have been presented for piezoelectric (Alghisi et al., 2017; Asthana and Khanna, 2020; Chen et al., 2017a; Khan et al., 2019) and triboelectric nanogenerators (Chen et al., 2018b; Fang et al., 2020; Harmon et al., 2020; Liu et al., 2020b; Niu et al., 2015; Qin et al. 2018, 2020; Zi et al., 2017). State-of-the-art PMCs for PEHs with various rectification techniques, architectures, and topologies have been discussed and compared (Brenes et al., 2020; Dell'Anna et al., 2018).

8.4. Biocompatibility

Biocompatibility is an essential element for wearable and implantable PEHs or self-powered sensors, as summarized in several recent reviews (Chorsi et al., 2019; Jeong et al., 2017; Kim et al., 2020a; Li et al., 2020b; Todaro et al., 2018; Wei et al., 2018; Zhang et al., 2020c). While many inorganic piezoelectric materials (e.g., $BaTiO_3$, GaN, and AlN) are biocompatible, lead-based piezoelectric materials such as PZT are not directly suitable for biological applications, mainly because the toxic Pb causes severe chronic poisoning and pain. A commonly used method for addressing this challenge is to encapsulate the device with biomaterials. For example, the implanted PZT-based PEHs proposed have been encapsulated with biocompatible materials to isolate them from bodily tissue and fluids for avoiding the risk of the immune response (Dagdeviren et al., 2014; Lu et al., 2015). On the other hand, most organic piezoelectric materials with intrinsic biocompatibility make them more applicable to bio-integrated devices. However, their relatively weaker piezoelectricity compared to their inorganic counterparts limits their potential. New classes of piezoelectric composite materials have partially addressed this issue by combining the merits of both organic and inorganic materials. Nevertheless, it is still significant to investigate the synthesis of lead-free materials with high piezoelectricity as well as effective encapsulation strategies for long-term biocompatibility.

9. Conclusion and outlook

This paper reviews the recent developments of flexible and stretchable piezoelectric energy harvesters and sensors. These stretchable materials and structures enhance stretchability and even increase piezoelectricity for piezoelectric devices. These devices are discussed along with their applications in wearable and implantable forms. In conclusion, flexible and stretchable piezoelectric energy harvesters with high piezoelectricity have demonstrated a high potential to maintain the sustainable operation of wearable and implantable devices. *In vivo* experiments performed with animals indicate that electrical output harvested from the motion of internal organs is sufficient for low-power consumption implanted electronics (e.g., pacemakers, blood pressure sensors, among others). The current key technologies for developing flexible and stretchable piezoelectric energy harvesters and sensors mainly include (1) novel material synthesis, (2) stretchable structural designs, and (3) advanced manufacturing approaches. While advanced material synthesis technologies can help prepare intrinsically stretchable piezoelectric materials, stretchable structures can enable stretchable piezoelectric devices based on brittle materials. The representative stretchable structures include wavy/buckled geometries, fractal layouts, and kirigami configurations, among others. The advanced manufacturing approaches may also combine lithographical processes and transfer printing techniques with newly emerged additive manufacturing approaches to integrate stretchable materials and structures to open up new opportunities for stretchable devices. Although great strides have been made in this burgeoning area of flexible and stretchable piezoelectric energy harvesters and self-powered sensors, there still exist challenges and thus opportunities for future developments, with a few represented ones outlined in the following.

(1) Although stretchable piezoelectric energy harvesters and self-powered sensors have demonstrated great potential for bio-integrated devices, several obstacles still exist before taking these devices from the research laboratory to the marketplace. One of the most important considerations in commercialization is the reliability and durability of the potential product. Therefore, functional failures need to be systematically studied, which includes debonding between adjacent layers, fatigue damage, binding force failure at interphases, among others. In addition to cheaper materials, scalable manufacturing methods are also desirable to fabricate stretchable piezoelectric devices.
(2) The frequency of human activities is much smaller than that of the PEHs. Therefore, various frequency up-conversion designs have been proposed and studied, which helps induce high-frequency mechanical vibration from low-frequency human activities for more efficient energy harvesting. However, they are often bulky and not flexible, thereby significantly reducing the level of comfort when used in wearable electronics. It could be even more challenging to apply them for implantable devices. Thus, it is of significant interest to apply stretchable structures to design stretchable frequency up-conversion components for the future piezoelectric energy harvesters and self-powered sensors.
(3) Most of the theoretical studies of piezoelectric energy harvesters and self-powered sensors focus on the buckled structures. While widely used, they cannot be directly applied for the other highly stretchable but more complicated structures such as kirigami and helical structures. Developing theoretical models to analyze the coupled mechanical and electrical behavior of these device structures will greatly contribute to the structural optimization and performance improvement of stretchable piezoelectric devices.
(4) Novel piezoelectric materials with new functional properties can open up application opportunities. For instance, the application of transparent piezoelectric materials ranges from photoacoustic imaging transducers to transparent actuators for haptic applications. One challenge for conventional transparent piezoelectric materials is that the high piezoelectricity only appears when the domain size is very small. On the other hand, it is difficult to simultaneously achieve transparency and high piezoelectricity. Both of these challenges have been addressed by

using an alternating current electric field to engineer the domain structures of originally opaque rhombohedral $Pb(Mg_{1/3}Nb_{2/3})O_3$–$PbTiO_3$ crystals (Qiu et al., 2020). This transparent ferroelectric crystal with ultrahigh piezoelectricity exhibits near-perfect transparency, ultrahigh piezoelectricity, a large electro-optical coefficient, and an excellent electromechanical coupling factor (Fig. 8A). Exploring this transparent or other novel piezoelectric materials may result in expanded opportunities for stretchable piezoelectric devices, including piezoelectric energy harvesters, self-powered sensors, medical imaging systems, and invisible robotic devices.

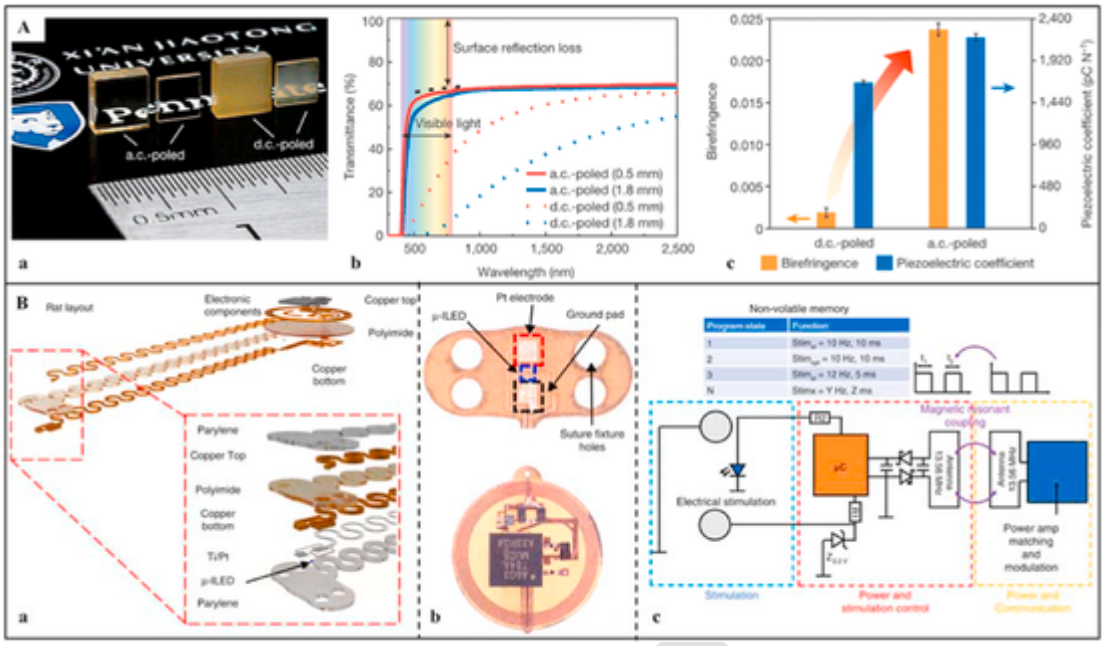

Fig. 8. (**A**) Property comparisons of the AC poled and conventional DC poled [001]-oriented PMN-28PT crystals. (a) Photograph of AC-poled samples with a thickness of 0.5 mm and DC-poled samples with a thickness of 1.8 mm. The AC-poled samples are transparent. (b) Comparison of the light transmittance of the AC- and DC-poled PMN-28PT crystals. The AC-poled sample has much higher light transmittance (close to its theoretical limit) than that of the DC-poled sample, especially in the visible-light spectrum. (c) Birefringence and piezoelectric coefficient of the AC- and DC-poled PMN-28PT crystals. The AC poling enables the increase in both the birefringence and piezoelectric coefficient for PMN-PT crystals. Reproduced with permission from (Qiu et al., 2020); Copyright 2020, Springer Nature. (**B**) Schematic illustration of the designed wireless, battery-free, and fully implantable pacemakers with capabilities of electrical and optical stimulation. (a) Exploded view of the layered designs of the proposed device configured for rats and mice. (b) Optical micrograph of the stimulation electrode for electrical and optical stimulations, harvester (receiver), and stimulation control unit. (c) Schematic illustration of the electrical working principles. The radio frequency power is harvested based on magnetic resonant coupling via receiving and transmitting antennas. Reproduced with permission from (Gutruf et al., 2019).

(5) Multifunctional medical devices are highly desirable for future healthcare applications. While it is beneficial to integrate multimodal sensors, the power consumption of the integrated device will also increase. The output power from the flexible and stretchable energy harvester may not be sufficient to meet the increasing energy requirements. Increasing the output power can be possible with the use of high-piezoelectric materials such as the 3D piezoelectric polymer composites based on a 3D piezoceramic skeleton (Zhang et al., 2018a). The designed 3D piezoceramic skeleton enables effective stress transfer in the polymer composites to greatly improve the piezoelectric performance. In another example, the polymer composite based on the 3D piezoceramic skeleton using rare-earth samarium-doped PMN-PT exhibits greatly enhanced energy harvesting output (Zhang et al., 2018b). The maximum instantaneous power density reaches 11.5 μW/cm^2, which is about 16 times higher than that of the conventional nanoparticle-based composite. Combining new piezoelectric materials with stretchable structures can also present promising solutions for novel stretchable energy harvesters. Additionally, other performance metrics, including stability and durability, also need to be optimized and improved to meet the increasing demands in practical applications.

(6) Animal models offer optimal versatility to investigate cardiovascular diseases with varying phenotypes or genotypes. However, current methods for providing cardiac stimuli almost exclusively use a physical tether. These methods are limiting the *in vivo* studies to anesthetized animals. Because they are not suitable for conscious, freely moving animal models, the lack of capabilities for long-term *in vivo* investigations hinders our overall understanding of the pathogenesis of atrial fibrillation and heart failure. One solution for this challenging issue is to use wireless, battery-free, fully implantable multimodal and multisite pacemakers based on serpentine structure (Fig. 8B–a) (Gutruf et al., 2019). This device supports optical and electrical multisite stimulation induced by a battery-free operation that exploits wireless magnetic resonant coupling (Fig. 8B-bc). The receiving antenna within the implanted device harvests radio frequency power from the transmitting antenna that encircles the experimental arena via a magnetic resonant coupling. The harvested energy provides a sufficient and stable power supply to the device for electrical and optical stimulation. The tether-free nature enables the investigations with freely moving, fully conscious subjects in isolation or social groups. The wirelessly powered multiple battery-free pacemakers greatly improve the quality of resynchronization therapy. Therefore, the combination of wearable piezoelectric harvesters with a high power density and wireless charging technology represents an important impetus for the future development of implantable medical devices to significantly increase their operational lifetime.

Author contributions

H.Z., Y.Z., Y.Q., H.W., W.Q, Y.L., Q.Y, and H.C. wrote the manuscript and assembled figures. H.C. led the preparation of the manuscript and contributed to editorial modifications of the overall text.

Declaration of competing interest

The authors declare that they have no known competing financial interests or personal relationships that could have appeared to influence the work reported in this paper.

Acknowledgment

Acknowledgmentis made to the start-up fund at The Pennsylvania State University, National Science Foundation (NSF) (Grant No. ECCS-1933072), and the donors of The American Chemical Society Petro-

leum Research Fund (Grant No. 59021-DNI7) for support of this research. The partial support from various seed grants at Penn State (H.C.), the Commonwealth Campuses & Shared Facilities & Collaboration Development Program at Penn State (Y.L. and H.C.), and NSFC (Grant No. 11872308 to Q.Y.) is also acknowledged. The authors also acknowledge the insightful edits from Lo Verso Jr., Antonino at The Pennsylvania State University, and Patrick Glynn at State College.

References

Abinnas, N, Baskaran, P, Harish, S, Ganesh, R S, Navaneethan, M, Nisha, K D, Ponnusamy, S, Muthamizhchelvan, C, Ikeda, H, Hayakawa, Y, 2017. Appl. Surf. Sci. 418, 362–368.
Ahn, S, Choe, A, Park, J, Kim, H, Son, J G, Lee, S-S, Park, M, Ko, H, 2015. J. Mater. Chem. C 3 (10), 2319–2325.
Ahn, Y, Song, S, Yun, K-S, 2015. Smart Mater. Struct. 24 (7), 075002.
Alghisi, D, Ferrari, V, Ferrari, M, Crescini, D, Touati, F, Mnaouer, A B, 2017. Sensor Actuator Phys. 264, 234–246.
Alhasssan, Z A, Burezq, Y S, Nair, R, Shehata, N, 2018. J. Nanomater. 2018, 8164185.
Ali, F, Raza, W, Li, X, Gul, H, Kim, K-H, 2019. Nanomater. Energy 57, 879–902.
Almusallam, A, Luo, Z, Komolafe, A, Yang, K, Robinson, A, Torah, R, Beeby, S, 2017. Nanomater. Energy 33, 146–156.
An, T, Cheng, W, 2018. J. Mater. Chem. 6 (32), 15478–15494.
Asthana, P, Khanna, G, 2020. Microelectron. J. 98, 104734.
Azimi, B, Milazzo, M, Lazzeri, A, Berrettini, S, Uddin, M J, Qin, Z, Buehler, M J, Danti, S, 2020. Advanced Healthcare Materials 9 (1), 1901287.
Bandodkar, A J, Nuñez-Flores, R, Jia, W, Wang, J, 2015. Adv. Mater. 27 (19), 3060–3065.
Baniasadi, M, Huang, J, Xu, Z, Moreno, S, Yang, X, Chang, J, Quevedo-Lopez, M A, Naraghi, M, Minary-Jolandan, M, 2015. ACS Appl. Mater. Interfaces 7 (9), 5358–5366.
Brenes, A, Morel, A, Juillard, J, Lefeuvre, E, Badel, A, 2020. Smart Mater. Struct. 29 (3), 033001.
Bussy, C, Boutouyrie, P, Lacolley, P, Challande, P, Laurent, S, 2000. Hypertension 35 (5), 1049–1054.
Chen, G, Li, Y, Bick, M, Chen, J, 2020. Chem. Rev. 120 (8), 3668–3720.
Chen, G, Matsuhisa, N, Liu, Z, Qi, D, Cai, P, Jiang, Y, Wan, C, Cui, Y, Leow, W R, Liu, Z, Gong, S, Zhang, K-Q, Cheng, Y, Chen, X, 2018. Adv. Mater. 30 (21), 1800129.
Chen, H, Bai, L, Li, T, Zhao, C, Zhang, J, Zhang, N, Song, G, Gan, Q, Xu, Y, 2018. Nanomater. Energy 46, 73–80.
Chen, J, Huang, Y, Zhang, N, Zou, H, Liu, R, Tao, C, Fan, X, Wang, Z L, 2016. Nature Energy 1 (10), 16138.
Chen, N, Jung, H J, Jabbar, H, Sung, T H, Wei, T, 2017. Sensor Actuator Phys. 254, 134–144.
Chen, X, 2017. Small Methods 1 (4), 1600029.
Chen, Y, Lu, B, Chen, Y, Feng, X, 2015. Sci. Rep. 5 (1), 11505.
Chen, Y, Lu, B, Ou, D, Feng, X, 2015. Science China physics. Mechanics & Astronomy 58 (9), 594601.
Chen, Y, Lu, S, Zhang, S, Li, Y, Qu, Z, Chen, Y, Lu, B, Wang, X, Feng, X, 2017. Science Advances 3 (12), e1701629.
Chen, Y, Zhang, Y, Yuan, F, Ding, F, Schmidt, O G, 2017. Advanced Electronic Materials 3 (3), 1600540.
Cheng, H, Yi, N, 2017. Phys. Scripta 92 (1), 013001.
Cheng, T, Zhang, Y, Lai, W-Y, Huang, W, 2015. Adv. Mater. 27 (22), 3349–3376.
Cheng, X, Xue, X, Ma, Y, Han, M, Zhang, W, Xu, Z, Zhang, H, Zhang, H, 2016. Nanomater. Energy 22, 453–460.
Choi, M, Murillo, G, Hwang, S, Kim, J W, Jung, J H, Chen, C-Y, Lee, M, 2017. Nanomater. Energy 33, 462–468.
Choi, S, Han, S I, Kim, D, Hyeon, T, Kim, D-H, 2019. Chem. Soc. Rev. 48 (6), 1566–1595.
Choi, W, Choi, K, Yang, G, Kim, J C, Yu, C, 2016. Polym. Test. 53, 143–148.
Chorsi, M T, Curry, E J, Chorsi, H T, Das, R, Baroody, J, Purohit, P K, Ilies, H, Nguyen, T D, 2019. Adv. Mater. 31 (1), 1802084.
Chou, X, Zhu, J, Qian, S, Niu, X, Qian, J, Hou, X, Mu, J, Geng, W, Cho, J, He, J, Xue, C, 2018. Nanomater. Energy 53, 550–558.
Chu, X, Zhang, H, Su, H, Liu, F, Gu, B, Huang, H, Zhang, H, Deng, W, Zheng, X, Yang, W, 2018. Chem. Eng. J. 349, 168–175.
Chun, J, Kang, N-R, Kim, J-Y, Noh, M-S, Kang, C-Y, Choi, D, Kim, S-W, Lin Wang, Z, Min Baik, J, 2015. Nanomater. Energy 11, 1–10.
Chun, K-Y, Son, Y J, Jeon, E-S, Lee, S, Han, C-S, 2018. Adv. Mater. 30 (12), 1706299.
Dagdeviren, C, Joe, P, Tuzman, O L, Park, K-I, Lee, K J, Shi, Y, Huang, Y, Rogers, J A, 2016. Extreme Mechanics Letters 9, 269–281.
Dagdeviren, C, Yang, B D, Su, Y, Tran, P L, Joe, P, Anderson, E, Xia, J, Doraiswamy, V, Dehdashti, B, Feng, X, Lu, B, Poston, R, Khalpey, Z, Ghaffari, R, Huang, Y, Slepian, M J, Rogers, J A, 2014. Proc. Natl. Acad. Sci. Unit. States Am. 111 (5), 1927–1932.
Dahiya, A S, Morini, F, Boubenia, S, Nadaud, K, Alquier, D, Poulin-Vittrant, G, 2018. Advanced Materials Technologies 3 (2), 1700249.
Dammers, R, Stifft, F, Tordoir, J H M, Hameleers, J M M, Hoeks, A P G, Kitslaar, P J E H M, 2003. J. Appl. Physiol. 94 (2), 485–489.
Das, S, Biswal, A K, Parida, K, Choudhary, R N P, Roy, A, 2018. Appl. Surf. Sci. 428, 356–363.
Dell'Anna, F, Dong, T, Li, P, Wen, Y, Yang, Z, Casu, M R, Azadmehr, M, Berg, Y, 2018. IEEE Circ. Syst. Mag. 18 (3), 27–48.
Ding, Y, Duan, Y, Huang, Y, 2015. Energy Technol. 3 (4), 351–358.
Dong, K, Peng, X, Wang, Z L, 2020. Adv. Mater. 32 (5), 1902549.
Dong, L, Wen, C, Liu, Y, Xu, Z, Closson, A B, Han, X, Escobar, G P, Oglesby, M, Feldman, M, Chen, Z, Zhang, J X J, 2019. Advanced Materials Technologies 4 (1), 1800335.
Dong, W, Cheng, X, Xiong, T, Wang, X, 2019. Biomed. Microdevices 21 (1), 6.
Duan, Y, Ding, Y, Bian, J, Xu, Z, Yin, Z, Huang, Y, 2017. Polymers 9 (12), 714.
El Achaby, M, Arrakhiz, F Z, Vaudreuil, S, Essassi, E M, Qaiss, A, 2012. Appl. Surf. Sci. 258 (19), 7668–7677.
Fan, Y J, Yu, P T, Liang, F, Li, X, Li, H, Liu, L, Cao, J W, Zhao, X J, Wang, Z L, Zhu, G, 2020. Nanoscale 12, 16053–16062.
Fang, C, Tong, T, Bu, T, Cao, Y, Xu, S, Qi, Y, Zhang, C, 2020. Advanced Intelligent Systems 2 (2), 1900129.
Feng, X, Yang, B D, Liu, Y, Wang, Y, Dagdeviren, C, Liu, Z, Carlson, A, Li, J, Huang, Y, Rogers, J A, 2011. ACS Nano 5 (4), 3326–3332.
Fu, H, Yeatman, E M, 2017. Energy 125, 152–161.
Fu, Y, He, H, Zhao, T, Dai, Y, Han, W, Ma, J, Xing, L, Zhang, Y, Xue, X, 2018. Nano-Micro Lett. 10 (4), 76.
Gao, W, Emaminejad, S, Nyein, H Y Y, Challa, S, Chen, K, Peck, A, Fahad, H M, Ota, H, Shiraki, H, Kiriya, D, Lien, D-H, Brooks, G A, Davis, R W, Javey, A, 2016. Nature 529, 509–514.
Gong, S, Zhang, B, Zhang, J, Wang, Z L, Ren, K, 2020. Adv. Funct. Mater. 30 (14), 1908724.
Güder, F, Ainla, A, Redston, J, Mosadegh, B, Glavan, A, Martin, T J, Whitesides, G M, 2016. Angew. Chem. Int. Ed. 55 (19), 5727–5732.
Guillon, O, Thiebaud, F, Perreux, D, 2002. Int. J. Fract. 117 (3), 235–246.
Guo, R, Guo, Y, Duan, H, Li, H, Liu, H, 2017. ACS Appl. Mater. Interfaces 9 (9), 8271–8279.
Gutruf, P, Yin, R T, Lee, K B, Ausra, J, Brennan, J A, Qiao, Y, Xie, Z, Peralta, R, Talarico, O, Murillo, A, Chen, S W, Leshock, J P, Haney, C R, Waters, E A, Zhang, C, Luan, H, Huang, Y, Trachiotis, G, Efimov, I R, Rogers, J A, 2019. Nat. Commun. 10 (1), 5742.
Hagood, N W, Chung, W H, Von Flotow, A, 1990. J. Intell. Mater. Syst. Struct. 1 (3), 327–354.
Han, M, Wang, H, Yang, Y, Liang, C, Bai, W, Yan, Z, Li, H, Xue, Y, Wang, X, Akar, B, Zhao, H, Luan, H, Lim, J, Kandela, I, Ameer, G A, Zhang, Y, Huang, Y, Rogers, J A, 2019. Nature Electronics 2 (1), 26–35.
Han, S, Kim, J, Won, S M, Ma, Y, Kang, D, Xie, Z, Lee, K-T, Chung, H U, Banks, A, Min, S, Heo, S Y, Davies, C R, Lee, J W, Lee, C-H, Kim, B H, Li, K, Zhou, Y, Wei, C, Feng, X, Huang, Y, Rogers, J A, 2018. Sci. Transl. Med. 10 (435), eaan4950.
Harmon, W, Bamgboje, D, Guo, H, Hu, T, Wang, Z L, 2020. Nanomater. Energy 71, 104642.
He, Z, Gao, B, Li, T, Liao, J, Liu, B, Liu, X, Wang, C, Feng, Z, Gu, Z, 2019. ACS Sustain. Chem. Eng. 7 (1), 1745–1752.
Hong, S, Lee, J, Do, K, Lee, M, Kim, J H, Lee, S, Kim, D-H, 2017. Adv. Funct. Mater. 27 (48), 1704353.
Hou, X, Zhang, S, Yu, J, Cui, M, He, J, Li, L, Wang, X, Chou, X, 2020. Energy Technol. 8 (3), 1901242.
Hu, N, Chen, D, Wang, D, Huang, S, Trase, I, Grover, H M, Yu, X, Zhang, J X J, Chen, Z, 2018. Physical Review Applied 9 (2), 021002.
Hu, P, Yan, L, Zhao, C, Zhang, Y, Niu, J, 2018. Compos. Sci. Technol. 168, 327–335.
Hu, Y, Wang, Z L, 2015. Nanomater. Energy 14, 3–14.
Huang, S, Liu, Y, Zhao, Y, Ren, Z, Guo, C F, 2019. Adv. Funct. Mater. 29 (6), 1805924.
Huang, Y, Ding, Y, Bian, J, Su, Y, Zhou, J, Duan, Y, Yin, Z, 2017. Nanomater. Energy 40, 432–439.
Hwang, G-T, Park, H, Lee, J-H, Oh, S, Park, K-I, Byun, M, Park, H, Ahn, G, Jeong, C K, No, K, Kwon, H, Lee, S-G, Joung, B, Lee, K J, 2014. Adv. Mater. 26 (28), 4880–4887.
Isobe, M, Okumura, K, 2016. Sci. Rep. 6 (1), 24758.
Issa, A A, Al-Maadeed, M A, Luyt, A S, Ponnamma, D, Hassan, M K, 2017. C — Journal of Carbon Research 3 (4), 30.
Jeong, C K, Han, J H, Palneedi, H, Park, H, Hwang, G-T, Joung, B, Kim, S-G, Shin, H J, Kang, I-S, Ryu, J, Lee, K J, 2017. Apl. Mater. 5 (7), 074102.
Jeong, C K, Lee, J, Han, S, Ryu, J, Hwang, G-T, Park, D Y, Park, J H, Lee, S S, Byun, M, Ko, S H, Lee, K J, 2015. Adv. Mater. 27 (18), 2866–2875.
Jeong, J W, Kim, M K, Cheng, H, Yeo, W H, Huang, X, Liu, Y, Zhang, Y, Huang, Y, Rogers, J A, 2014. Adv Healthc Mater 3 (5), 642–648.
Ji, B, Xie, Z, Hong, W, Jiang, C, Guo, Z, Wang, L, Wang, X, Yang, B, Liu, J, 2020. Journal of Materiomics 6 (2), 330–338.
Jung, J, Cho, H, Yuksel, R, Kim, D, Lee, H, Kwon, J, Lee, P, Yeo, J, Hong, S, Unalan, H E, Han, S, Ko, S H, 2019. Nanoscale 11 (43), 20356–20378.
Kang, H B, Han, C S, Pyun, J C, Ryu, W H, Kang, C-Y, Cho, Y S, 2015. Compos. Sci. Technol. 111, 1–8.
Kang, S-K, Murphy, R K J, Hwang, S-W, Lee, S M, Harburg, D V, Krueger, N A, Shin, J, Gamble, P, Cheng, H, Yu, S, Liu, Z, McCall, J G, Stephen, M, Ying, H, Kim, J, Park, G, Webb, R C, Lee, C H, Chung, S, Wie, D S, Gujar, A D, Vemulapalli, B, Kim, A H, Lee, K-M, Cheng, J, Huang, Y, Lee, S H, Braun, P V, Ray, W Z, Rogers, J A, 2016. Nature 530 (7588), 71–76.
Kar, E, Bose, N, Dutta, B, Banerjee, S, Mukherjee, N, Mukherjee, S, 2019. Energy Convers. Manag. 184, 600–608.
Kathpalia, B, Tan, D, Stern, I, Erturk, A, 2017. Smart Mater. Struct. 27 (1), 015024.
Khan, M B, Kim, D H, Han, J H, Saif, H, Lee, H, Lee, Y, Kim, M, Jang, E, Hong, S K, Joe, D J, Lee, T-I, Kim, T-S, Lee, K J, Lee, Y, 2019. Nanomater. Energy 58, 211–219.
Kim, D, Han, S A, Kim, J H, Lee, J-H, Kim, S-W, Lee, S-W, 2020. Adv. Mater. 32 (14), 1906989.
Kim, D C, Shim, H J, Lee, W, Koo, J H, Kim, D-H, 2020. Adv. Mater. 32 (15), 1902743.
Kim, H, Priya, S, Stephanou, H, Uchino, K, 2007. IEEE Trans. Ultrason. Ferroelectrics Freq. Contr. 54 (9), 1851–1859.
Kim, H W, Batra, A, Priya, S, Uchino, K, Markley, D, Newnham, R E, Hofmann, H F, 2004. Jpn. J. Appl. Phys. 43 (9A), 6178–6183.
Kim, K, Kim, J, Hyun, B G, Ji, S, Kim, S-Y, Kim, S, An, B W, Park, J-U, 2015. Nanoscale 7 (35), 14577–14594.
Kim, K, Song, G, Park, C, Yun, K-S, 2017. Sensors 17 (11), 2582.
Kim, K, Yun, K-S, 2019. International Journal of Precision Engineering and Manufacturing-Green Technology 6 (4), 699–710.
Kim, M, Yun, K-S, 2017. Micromachines 8 (4), 115.
Kim, S-R, Yoo, J-H, Cho, Y S, Park, J-W, 2019. Mater. Res. Express 6 (8), 086311.

Kim, S, Lee, J, Choi, B, 2015. IEEE Sensor. J. 15 (11), 6077–6078.
Kim, Y, Kweon, O Y, Won, Y, Oh, J H, 2019. Macromol. Res. 27 (7), 625–639.
Kim, Y, Lee, K Y, Hwang, S K, Park, C, Kim, S-W, Cho, J, 2014. Adv. Funct. Mater. 24 (40), 6262–6269.
Kon, S, Horowitz, R, 2008. IEEE Sensor. J. 8 (12), 2027–2035.
Kong, N, Ha, D S, Erturk, A, Inman, D J, 2010. J. Intell. Mater. Syst. Struct. 21 (13), 1293–1302.
Ku, N-J, Liu, G, Wang, C-H, Gupta, K, Liao, W-S, Ban, D, Liu, C-P, 2017. Nanoscale 9 (37), 14039–14046.
Kuang, Y, Yang, Z, Zhu, M, 2016. Smart Mater. Struct. 25 (8), 085029.
Kumar, R, Kumar, G, Al-Dossary, O, Umar, A, 2015. Materials Express 5 (1), 3–23.
Kunin, V, Yang, S, Cho, Y, Deymier, P, Srolovitz, D J, 2016. Extreme Mechanics Letters 6, 103–114.
Lagomarsini, C, Jean-Mistral, C, Lombardi, G, Sylvestre, A, 2019. Smart Mater. Struct. 28 (3), 035003.
Lamoureux, A, Lee, K, Shlian, M, Forrest, S R, Shtein, M, 2015. Nat. Commun. 6 (1), 8092.
Lan, C, Qin, W, Deng, W, 2015. Appl. Phys. Lett. 107 (9), 093902.
Larson, C, Peele, B, Li, S, Robinson, S, Totaro, M, Beccai, L, Mazzolai, B, Shepherd, R, 2016. Science 351 (6277), 1071–1074.
Lee, H, Hong, S, Lee, J, Suh, Y D, Kwon, J, Moon, H, Kim, H, Yeo, J, Ko, S H, 2016. ACS Appl. Mater. Interfaces 8 (24), 15449–15458.
Lee, H, Kim, I, Kim, M, Lee, H, 2016. Nanoscale 8 (4), 1789–1822.
Lee, J-H, Yoon, H-J, Kim, T Y, Gupta, M K, Lee, J H, Seung, W, Ryu, H, Kim, S-W, 2015. Adv. Funct. Mater. 25 (21), 3203–3209.
Lee, J, Llerena Zambrano, B, Woo, J, Yoon, K, Lee, T, 2020. Adv. Mater. 32 (5), 1902532.
Lee, S, Bae, S-H, Lin, L, Yang, Y, Park, C, Kim, S-W, Cha, S N, Kim, H, Park, Y J, Wang, Z L, 2013. Adv. Funct. Mater. 23 (19), 2445–2449.
Lee, S, Hinchet, R, Lee, Y, Yang, Y, Lin, Z-H, Ardila, G, Montès, L, Mouis, M, Wang, Z L, 2014. Adv. Funct. Mater. 24 (8), 1163–1168.
Lee, S P, Ha, G, Wright, D E, Ma, Y, Sen-Gupta, E, Haubrich, N R, Branche, P C, Li, W, Huppert, G L, Johnson, M, Mutlu, H B, Li, K, Sheth, N, Wright, J A, Huang, Y, Mansour, M, Rogers, J A, Ghaffari, R, 2018. npj Digital Medicine 1 (1), 2.
Lee, Y-Y, Kang, H-Y, Gwon, S H, Choi, G M, Lim, S-M, Sun, J-Y, Joo, Y-C, 2016. Adv. Mater. 28 (8), 1636–1643.
Lee, Y, Park, J, Cho, S, Shin, Y-E, Lee, H, Kim, J, Myoung, J, Cho, S, Kang, S, Baig, C, Ko, H, 2018. ACS Nano 12 (4), 4045–4054.
Lesieutre, G A, Ottman, G K, Hofmann, H F, 2004. J. Sound Vib. 269 (3), 991–1001.
Li, H, Ma, Y, Liang, Z, Wang, Z, Cao, Y, Xu, Y, Zhou, H, Lu, B, Chen, Y, Han, Z, Cai, S, Feng, X, 2020. National Science Review 7 (5), 849–862.
Li, H, Xu, Y, Li, X, Chen, Y, Jiang, Y, Zhang, C, Lu, B, Wang, J, Ma, Y, Chen, Y, Huang, Y, Ding, M, Su, H, Song, G, Luo, Y, Feng, X, 2017. Advanced Healthcare Materials 6 (9), 1601013.
Li, J, Long, Y, Yang, F, Wang, X, 2020. Curr. Opin. Solid State Mater. Sci. 24 (1), 100806.
Li, J, Niu, J, Li, X, Zhou, J, Hu, Z, Guo, W, 2020. Science China Technological Sciences. doi:10.1007/s11431-019-1591-7.
Li, J, Yin, J, Yang, C, Li, N, Feng, Y, Liu, Y, Zhao, H, Li, Y, Zhu, C, Yue, D, Su, B, Liu, X, 2019. J. Polym. Sci. B Polym. Phys. 57 (10), 574–583.
Li, J, Zhao, C, Xia, K, Liu, X, Li, D, Han, J, 2019. Appl. Surf. Sci. 463, 626–634.
Li, S, Han, M, Rogers, J A, Zhang, Y, Huang, Y, Wang, H, 2019. J. Mech. Phys. Solid. 125, 736–748.
Li, Z, Zheng, Q, Wang, Z L, Li, Z, 2020. Research 2020, 8710686.
Li, Z, Zhu, G, Yang, R, Wang, A C, Wang, Z L, 2010. Adv. Mater. 22 (23), 2534–2537.
Liang, J, Wang, S, Yu, H, Zhao, X, Wang, H, Tong, Y, Tang, Q, Liu, Y, 2020. Sustainable Energy & Fuels 4 (6), 2718–2726.
Liang, J R, Liao, W H, 2009. J. Intell. Mater. Syst. Struct. 20 (5), 515–527.
Liao, Y, Liang, J, 2018. Smart Mater. Struct. 27 (7), 075053.
Liao, Y, Sodano, H A, 2008. Smart Mater. Struct. 17 (6), 065026.
Liao, Y, Sodano, H A, 2009. J. Intell. Mater. Syst. Struct. 20 (5), 505–514.
Lim, J-E, Lee, D-Y, Kim, H-K, 2018. ECS Journal of Solid State Science and Technology 7 (9), 468–472.
Lim, M-H, Kang, K, Kim, H-G, Kim, I-D, Choi, Y, Tuller, H L, 2006. Appl. Phys. Lett. 89 (20), 202908.
Liu, H, Zhong, J, Lee, C, Lee, S-W, Lin, L, 2018. Appl. Phys. Rev. 5 (4), 041306.
Liu, K, Kong, B, Liu, W, Sun, Y, Song, M-S, Chen, J, Liu, Y, Lin, D, Pei, A, Cui, Y, 2018. Joule 2 (9), 1857–1865.
Liu, K, Yao, Y, Lv, T, Li, H, Li, N, Chen, Z, Qian, G, Chen, T, 2020. J. Power Sources 446, 227355.
Liu, W, Chen, J, Chen, Z, Liu, K, Zhou, G, Sun, Y, Song, M-S, Bao, Z, Cui, Y, 2017. Advanced Energy Materials 7 (21), 1701076.
Liu, W, Chen, Z, Zhou, G, Sun, Y, Lee, H R, Liu, C, Yao, H, Bao, Z, Cui, Y, 2016. Adv. Mater. 28 (18), 3578–3583.
Liu, W, Wang, Z, Wang, G, Zeng, Q, He, W, Liu, L, Wang, X, Xi, Y, Guo, H, Hu, C, Wang, Z L, 2020. Nat. Commun. 11 (1), 1883.
Liu, Y, Zhao, L, Wang, L, Zheng, H, Li, D, Avila, R, Lai, K W C, Wang, Z, Xie, Z, Zi, Y, Yu, X, 2019. Advanced Materials Technologies 4 (12), 1900744.
Liu, Z, Ju, K, Wang, Z, Li, W, Ke, H, He, J, 2019. Nanoscale Research Letters 14 (1), 310.
Liu, Z, Zhang, S, Jin, Y M, Ouyang, H, Zou, Y, Wang, X X, Xie, L X, Li, Z, 2017. Semicond. Sci. Technol. 32 (6), 064004.
Lou, Z, Wang, L, Jiang, K, Wei, Z, Shen, G, 2020. Mater. Sci. Eng. R Rep. 140, 100523.
Lu, B, Chen, Y, Ou, D, Chen, H, Diao, L, Zhang, W, Zheng, J, Ma, W, Sun, L, Feng, X, 2015. Sci. Rep. 5 (1), 16065.
Lü, C, Zhang, Y, Zhang, H, Zhang, Z, Shen, M, Chen, Y, 2019. Energy Convers. Manag. 182, 34–40.
Lund, A, Rundqvist, K, Nilsson, E, Yu, L, Hagström, B, Müller, C, 2018. npj Flexible Electronics 2 (1), 9.
Lyu, J, Hammig, M D, Liu, L, Xu, L, Chi, H, Uher, C, Li, T, Kotov, N A, 2017. Appl. Phys. Lett. 111 (16), 161901.
Ma, T, Wang, Y, Tang, R, Yu, H, Jiang, H, 2013. J. Appl. Phys. 113 (20), 204503.
Ma, X, Wilson, A, Rahn, C D, Trolier-McKinstry, S, 2016. J. Vib. Acoust. 138 (2), 021005.
Ma, Y, Choi, J, Hourlier-Fargette, A, Xue, Y, Chung, H U, Lee, J Y, Wang, X, Xie, Z, Kang, D, Wang, H, Han, S, Kang, S-K, Kang, Y, Yu, X, Slepian, M J, Raj, M S, Model, J B, Feng, X, Ghaffari, R, Rogers, J A, Huang, Y, 2018. Proc. Natl. Acad. Sci. Unit. States Am. 115 (44), 11144–11149.
Maity, K, Mandal, D, 2018. ACS Appl. Mater. Interfaces 10 (21), 18257–18269.
Mao, Y, Zhao, P, McConohy, G, Yang, H, Tong, Y, Wang, X, 2014. Advanced Energy Materials 4 (7), 1301624.
Meng, K, Zhao, S, Zhou, Y, Wu, Y, Zhang, S, He, Q, Wang, X, Zhou, Z, Fan, W, Tan, X, Yang, J, Chen, J, 2020. Matter 2 (4), 896–907.
Mokhtari, F, Foroughi, J, Zheng, T, Cheng, Z, Spinks, G M, 2019. J. Mater. Chem. 7 (14), 8245–8257.
Mondal, S, Paul, T, Maiti, S, Das, B K, Chattopadhyay, K K, 2020. Nanomater. Energy 74, 104870.
Ning, X, Wang, H, Yu, X, Soares, J A N T, Yan, Z, Nan, K, Velarde, G, Xue, Y, Sun, R, Dong, Q, Luan, H, Lee, C M, Chempakasseril, A, Han, M, Wang, Y, Li, L, Huang, Y, Zhang, Y, Rogers, J A, 2017. Adv. Funct. Mater. 27 (14), 1605914.
Ning, X, Wang, X, Zhang, Y, Yu, X, Choi, D, Zheng, N, Kim, D S, Huang, Y, Zhang, Y, Rogers, J A, 2018. Advanced Materials Interfaces 5 (13), 1800284.
Ning, X, Yu, X, Wang, H, Sun, R, Corman, R E, Li, H, Lee, C M, Xue, Y, Chempakasseril, A, Yao, Y, Zhang, Z, Luan, H, Wang, Z, Xia, W, Feng, X, Ewoldt, R H, Huang, Y, Zhang, Y, Rogers, J A, 2018. Science Advances 4 (9), eaat8313.
Niu, S, Wang, X, Yi, F, Zhou, Y S, Wang, Z L, 2015. Nat. Commun. 6 (1), 8975.
Niu, X, Jia, W, Qian, S, Zhu, J, Zhang, J, Hou, X, Mu, J, Geng, W, Cho, J, He, J, Chou, X, 2019. ACS Sustain. Chem. Eng. 7 (1), 979–985.
Noh, J-S, 2016. Polymers 8 (4), 123.
Owczarek, M, Hujsak, K A, Ferris, D P, Prokofjevs, A, Majerz, I, Szklarz, P, Zhang, H, Sarjeant, A A, Stern, C L, Jakubas, R, Hong, S, Dravid, V P, Stoddart, J F, 2016. Nat. Commun. 7 (1), 13108.
Pan, J-N, Qin, W-Y, Deng, W-Z, Zhou, H-L, 2019. Chin. Phys. B 28 (1), 017701.
Parangusan, H, Ponnamma, D, Al-Maadeed, M A A, 2018. Sci. Rep. 8 (1), 754.
Parangusan, H, Ponnamma, D, AlMaadeed, M A A, 2018. Soft Matter 14 (43), 8803–8813.
Park, D Y, Joe, D J, Kim, D H, Park, H, Han, J H, Jeong, C K, Park, H, Park, J G, Joung, B, Lee, K J, 2017. Adv. Mater. 29 (37), 1702308.
Park, J, Kim, M, Lee, Y, Lee, H S, Ko, H, 2015. Science Advances 1 (9), e1500661.
Park, S-H, Lee, H B, Yeon, S M, Park, J, Lee, N K, 2016. ACS Appl. Mater. Interfaces 8 (37), 24773–24781.
Pillatsch, P, Yeatman, E M, Holmes, A S, 2014. Sensor Actuator Phys. 206, 178–185.
Qi, Y, Kim, J, Nguyen, T D, Lisko, B, Purohit, P K, McAlpine, M C, 2011. Nano Lett. 11 (3), 1331–1336.
Qi, Y, McAlpine, M C, 2010. Energy Environ. Sci. 3 (9), 1275–1285.
Qian, S, Qin, L, He, J, Niu, X, Qian, J, Mu, J, Geng, W, Hou, X, Chou, X, 2019. Mater. Lett. 236, 96–100.
Qin, H, Cheng, G, Zi, Y, Gu, G, Zhang, B, Shang, W, Yang, F, Yang, J, Du, Z, Wang, Z L, 2018. Adv. Funct. Mater. 28 (51), 1805216.
Qin, H, Gu, G, Shang, W, Luo, H, Zhang, W, Cui, P, Zhang, B, Guo, J, Cheng, G, Du, Z, 2020. Nanomater. Energy 68, 104372.
Qiu, C, Wang, B, Zhang, N, Zhang, S, Liu, J, Walker, D, Wang, Y, Tian, H, Shrout, T R, Xu, Z, Chen, L-Q, Li, F, 2020. Nature 577 (7790), 350–354.
Rafsanjani, A, Bertoldi, K, 2017. Phys. Rev. Lett. 118 (8), 084301.
Ren, X, Pei, K, Peng, B, Zhang, Z, Wang, Z, Wang, X, Chan, P K L, 2016. Adv. Mater. 28 (24), 4832–4838.
Ryu, J, Kim, J, Oh, J, Lim, S, Sim, J Y, Jeon, J S, No, K, Park, S, Hong, S, 2019. Nanomater. Energy 55, 348–353.
Saravanakumar, B, Mohan, R, Thiyagarajan, K, Kim, S-J, 2013. RSC Adv. 3 (37), 16646–16656.
Shi, B, Li, Z, Fan, Y, 2018. Adv. Mater. 30 (44), 1801511.
Shi, K, Sun, B, Huang, X, Jiang, P, 2018. Nanomater. Energy 52, 153–162.
Shu, Y C, Lien, I C, 2006. Smart Mater. Struct. 15 (6), 1499–1512.
Shyu, T C, Damasceno, P F, Dodd, P M, Lamoureux, A, Xu, L, Shlian, M, Shtein, M, Glotzer, S C, Kotov, N A, 2015. Nat. Mater. 14 (8), 785–789.
Siddiqui, S, Lee, H B, Kim, D-I, Duy, L T, Hanif, A, Lee, N-E, 2018. Advanced Energy Materials 8 (2), 1701520.
Silva, C A, lv, J, Yin, L, Jeerapan, I, Innocenzi, G, Soto, F, Ha, Y-G, Wang, J, 2020. Adv. Funct. Mater. 30 (30), 2002041.
Sim, H J, Choi, C, Lee, C J, Kim, Y T, Spinks, G M, Lima, M D, Baughman, R H, Kim, S J, 2015. Adv. Eng. Mater. 17 (9), 1270–1275.
Singh, D, Choudhary, A, Garg, A, 2018. ACS Appl. Mater. Interfaces 10 (3), 2793–2800.
Son, W, Chun, S, Lee, J M, Lee, Y, Park, J, Suh, D, Lee, D W, Jung, H, Kim, Y-J, Kim, Y, Jeong, S M, Lim, S K, Choi, C, 2019. Nat. Commun. 10 (1), 426.
Song, J, Huang, Y, Xiao, J, Wang, S, Hwang, K C, Ko, H C, Kim, D-H, Stoykovich, M P, Rogers, J A, 2009. J. Appl. Phys. 105 (12), 123516.
Song, S, Yun, K-S, 2015. Smart Mater. Struct. 24 (4), 045008.
Song, Z, Wang, X, Lv, C, An, Y, Liang, M, Ma, T, He, D, Zheng, Y-J, Huang, S-Q, Yu, H, Jiang, H, 2015. Sci. Rep. 5 (1), 10988.
Su, Y, Dagdeviren, C, Li, R, 2015. Adv. Funct. Mater. 25 (33), 5320–5325.
Su, Y, Li, S, Li, R, Dagdeviren, C, 2015. Appl. Phys. Lett. 107 (4), 041905.
Su, Y, Ping, X, Yu, K J, Lee, J W, Fan, J A, Wang, B, Li, M, Li, R, Harburg, D V, Huang, Y, Yu, C, Mao, S, Shim, J, Yang, Q, Lee, P-Y, Armonas, A, Choi, K-J, Yang, Y, Paik, U, Chang, T, Dawidczyk, T J, Huang, Y, Wang, S, Rogers, J A, 2017. Adv. Mater. 29 (8), 1604989.
Su, Y, Wang, J, Wang, B, Yang, T, Yang, B, Xie, G, Zhou, Y, Zhang, S, Tai, H, Cai, Z, Chen, G, Jiang, Y, Chen, L-Q, Chen, J, 2020. ACS Nano 14 (5), 6067–6075.
Su, Y, Yang, T, Zhao, X, Cai, Z, Chen, G, Yao, M, Chen, K, Bick, M, Wang, J, Li, S, Xie, G, Tai, H, Du, X, Jiang, Y, Chen, J, 2020. Nanomater. Energy 74, 104941.
Sultana, A, Alam, M M, Garain, S, Sinha, T K, Middya, T R, Mandal, D, 2015. ACS Appl. Mater. Interfaces 7 (34), 19091–19097.
Sun, R, Carreira, S C, Chen, Y, Xiang, C, Xu, L, Zhang, B, Chen, M, Farrow, I, Scarpa, F, Rossiter, J, 2019. Advanced Materials Technologies 4 (5), 1900100.
Sun, R, Li, Q, Yao, J, Scarpa, F, Rossiter, J, 2020. Appl. Energy 264, 114615.

Sun, R, Zhang, B, Yang, L, Zhang, W, Farrow, I, Scarpa, F, Rossiter, J, 2018. Appl. Phys. Lett. 112 (25), 251904.
Sun, Y, Zeng, K, Li, T, 2020. Science China physics. Mechanics & Astronomy 63 (7), 278701.
Surmenev, R A, Orlova, T, Chernozem, R V, Ivanova, A A, Bartasyte, A, Mathur, S, Surmeneva, M A, 2019. Nanomater. Energy 62, 475–506.
Tang, Y, Lin, G, Yang, S, Yi, Y K, Kamien, R D, Yin, J, 2017. Adv. Mater. 29 (10), 1604262.
Todaro, M T, Guido, F, Algieri, L, Mastronardi, V M, Desmaële, D, Epifani, G, Vittorio, M D, 2018. IEEE Trans. Nanotechnol. 17 (2), 220–230.
Tsai, S-J, Lin, C-Y, Wang, C-L, Chen, J-W, Chen, C-H, Wu, C-L, 2017. Nanomater. Energy 37, 260–267.
Tybrandt, K, Khodagholy, D, Dielacher, B, Stauffer, F, Renz, A F, Buzsáki, G, Vörös, J, 2018. Adv. Mater. 30 (15), 1706520.
Vivekananthan, V, Chandrasekhar, A, Alluri, N R, Purusothaman, Y, Joong Kim, W, Kang, C-N, Kim, S-J, 2019. Mater. Lett. 249, 73–76.
Voiculescu, I, Li, F, Kowach, G, Lee, K-L, Mistou, N, Kastberg, R, 2019. Micromachines 10 (10), 661.
Wan, J, Xie, J, Kong, X, Liu, Z, Liu, K, Shi, F, Pei, A, Chen, H, Chen, W, Chen, J, Zhang, X, Zong, L, Wang, J, Chen, L-Q, Qin, J, Cui, Y, 2019. Nat. Nanotechnol. 14 (7), 705–711.
Wang, Z, Zhang, L, Duan, S, Jiang, H, Shen, J, Li, C, 2017. J. Mater. Chem. C 5 (34), 8714–8722.
Wang, Z L, Song, J, 2006. Science 312 (5771), 242–246.
Webb, R C, Bonifas, A P, Behnaz, A, Zhang, Y, Yu, K J, Cheng, H, Shi, M, Bian, Z, Liu, Z, Kim, Y S, Yeo, W H, Park, J S, Song, J, Li, Y, Huang, Y, Gorbach, A M, Rogers, J A, 2013. Nat. Mater. 12 (10), 938–944.
Wei, C, Jing, X, 2017. Renew. Sustain. Energy Rev. 74, 1–18.
Wei, H, Wang, H, Xia, Y, Cui, D, Shi, Y, Dong, M, Liu, C, Ding, T, Zhang, J, Ma, Y, Wang, N, Wang, Z, Sun, Y, Wei, R, Guo, Z, 2018. J. Mater. Chem. C 6 (46), 12446–12467.
Weng, W, Sun, Q, Zhang, Y, He, S, Wu, Q, Deng, J, Fang, X, Guan, G, Ren, J, Peng, H, 2015. Adv. Mater. 27 (8), 1363–1369.
Won, J, Mondal, S, Park, J, Wang, W, Lee, H, Kim, S, Shin, B, Sathi, S G, Nah, C, 2020. Polym. Compos. 41 (6), 2210–2223.
Wu, H, Tian, Y, Luo, H, Zhu, H, Duan, Y, Huang, Y, 2020. Advanced Materials Technologies 5 (8), 2000093.
Wu, S, Peng, S, Yu, Y, Wang, C-H, 2020. Advanced Materials Technologies 5 (2), 1900908.
Xin, Y, Zhu, J, Sun, H, Xu, Y, Liu, T, Qian, C, 2018. Ferroelectrics 526 (1), 140–151.
Xu, J, Tan, Z, Zeng, W, Chen, G, Wu, S, Zhao, Y, Ni, K, Tao, Z, Ikram, M, Ji, H, Zhu, Y, 2016. Adv. Mater. 28 (26), 5222–5228.
Xu, L, Shyu, T C, Kotov, N A, 2017. ACS Nano 11 (8), 7587–7599.
Xu, S-M, Liang, X, Wu, X-Y, Zhao, S-L, Chen, J, Wang, K-X, Chen, J-S, 2019. Nat. Commun. 10 (1), 5810.
Xu, S, Yeh, Y-w, Poirier, G, McAlpine, M C, Register, R A, Yao, N, 2013. Nano Lett. 13 (6), 2393–2398.
Xue, Z, Song, H, Rogers, J A, Zhang, Y, Huang, Y, 2020. Adv. Mater. 32 (15), 1902254.
Yan, C, Gao, Y, Zhao, S, Zhang, S, Zhou, Y, Deng, W, Li, Z, Jiang, G, Jin, L, Tian, G, Yang, T, Chu, X, Xiong, D, Wang, Z, Li, Y, Yang, W, Chen, J, 2020. Nanomater. Energy 67, 104235.
Yan, J, Jeong, Y G, 2016. ACS Appl. Mater. Interfaces 8 (24), 15700–15709.
Yan, Z, Pan, T, Wang, D, Li, J, Jin, L, Huang, L, Jiang, J, Qi, Z, Zhang, H, Gao, M, Yang, W, Lin, Y, 2019. ACS Appl. Mater. Interfaces 11 (13), 12261–12271.
Yan, Z, Wang, B, Wang, K, Zhao, S, Li, S, Huang, Y, Wang, H, 2019. J. Appl. Mech. 87 (2), 024501.
Yang, L, Yi, N, Zhu, J, Cheng, Z, Yin, X, Zhang, X, Zhu, H, Cheng, H, 2020. J. Mater. Chem. 8 (14), 6487–6500.
Yang, R, Qin, Y, Li, C, Zhu, G, Wang, Z L, 2009. Nano Lett. 9 (3), 1201–1205.
Yeo, H G, Xue, T, Roundy, S, Ma, X, Rahn, C, Trolier-McKinstry, S, 2018. Adv. Funct. Mater. 28 (36), 1801327.
Yi, N, Cheng, Z, Li, H, Yang, L, Zhu, J, Zheng, X, Chen, Y, Liu, Z, Zhu, H, Cheng, H, 2020. In: Materials Today Physics, 100265. doi:10.1016/j.mtphys.2020.100265.
Yi, N, Cheng, Z, Yang, L, Edelman, G, Xue, C, Ma, Y, Zhu, H, Cheng, H, 2018. ACS Appl. Mater. Interfaces 10, 36664–36674.
Yi, N, Cui, H, Zhang, L G, Cheng, H, 2019. Acta Biomater. 95, 91–111.
Ylli, K, Hoffmann, D, Willmann, A, Becker, P, Folkmer, B, Manoli, Y, 2015. Smart Mater. Struct. 24 (2), 025029.
Yoon, S, Kim, H-K, 2020. Surf. Coating. Technol. 384, 125308.
Yu, H, Chung, C-C, Shewmon, N, Ho, S, Carpenter, J H, Larrabee, R, Sun, T, Jones, J L, Ade, H, O'Connor, B T, So, F, 2017. Adv. Funct. Mater. 27 (21), 1700461.
Yu, X, Mahajan, B K, Shou, W, Pan, H, 2017. Micromachines 8 (1), 7.
Zaarour, B, Zhu, L, Huang, C, Jin, X, 2020. Polym. Adv. Technol. 31 (7), 1449–1462.
Zaarour, B, Zhu, L, Jin, X, 2019. Mater. Res. Express 7 (1), 015008.
Zan, G, Wu, T, Hu, P, Zhou, Y, Zhao, S, Xu, S, Chen, J, Cui, Y, Wu, Q, 2020. Energy Storage Materials 28, 82–90.
Zang, X, Zhu, M, Li, X, Li, X, Zhen, Z, Lao, J, Wang, K, Kang, F, Wei, B, Zhu, H, 2015. Nanomater. Energy 15, 83–91.
Zeng, Z, Gai, L, Petitpas, A, Li, Y, Luo, H, Wang, D, Zhao, X, 2017. Sensor Actuator Phys. 265, 62–69.
Zhang, G, Zhao, P, Zhang, X, Han, K, Zhao, T, Zhang, Y, Jeong, C K, Jiang, S, Zhang, S, Wang, Q, 2018. Energy Environ. Sci. 11 (8), 2046–2056.
Zhang, H, Zhang, X-S, Cheng, X, Liu, Y, Han, M, Xue, X, Wang, S, Yang, F, A S, S, Zhang, H, Xu, Z, 2015. Nanomater. Energy 12, 296–304.
Zhang, J, Liu, D, Han, Q, Jiang, L, Shao, H, Tang, B, Lei, W, Lin, T, Wang, C H, 2019. Compos. B Eng. 175, 107157.
Zhang, M, Gao, T, Wang, J, Liao, J, Qiu, Y, Yang, Q, Xue, H, Shi, Z, Zhao, Y, Xiong, Z, Chen, L, 2015. Nanomater. Energy 13, 298–305.
Zhang, N, Huang, F, Zhao, S, Lv, X, Zhou, Y, Xiang, S, Xu, S, Li, Y, Chen, G, Tao, C, Nie, Y, Chen, J, Fan, X, 2020. Matter 2 (5), 1260–1269.
Zhang, Y, Chen, Y, Huang, J, Liu, Y, Peng, J, Chen, S, Song, K, Ouyang, X, Cheng, H, Wang, X, 2020. Lab Chip 20 (15), 2635–2645.
Zhang, Y, Jeong, C K, Wang, J, Sun, H, Li, F, Zhang, G, Chen, L-Q, Zhang, S, Chen, W, Wang, Q, 2018. Nanomater. Energy 50, 35–42.
Zhang, Y, Kim, H, Wang, Q, Jo, W, Kingon, A I, Kim, S-H, Jeong, C K, 2020. Nanoscale Advances 2, 3131–3149.
Zhang, Y, Wang, F, Ma, Y, Feng, X, 2019. Int. J. Solid Struct. 161, 55–63.
Zhao, S, Li, J, Cao, D, Zhang, G, Li, J, Li, K, Yang, Y, Wang, W, Jin, Y, Sun, R, Wong, C-P, 2017. ACS Appl. Mater. Interfaces 9 (14), 12147–12164.
Zhou, X, Parida, K, Halevi, O, Liu, Y, Xiong, J, Magdassi, S, Lee, P S, 2020. Nanomater. Energy 72, 104676.
Zhou, Y, He, J, Wang, H, Qi, K, Nan, N, You, X, Shao, W, Wang, L, Ding, B, Cui, S, 2017. Sci. Rep. 7 (1), 12949.
Zhou, Z, Chen, K, Li, X, Zhang, S, Wu, Y, Zhou, Y, Meng, K, Sun, C, He, Q, Fan, W, Fan, E, Lin, Z, Tan, X, Deng, W, Yang, J, Chen, J, 2020. Nature Electronics. doi:10.1038/s41928-020-0428-6.
Zhou, Z, Padgett, S, Cai, Z, Conta, G, Wu, Y, He, Q, Zhang, S, Sun, C, Liu, J, Fan, E, Meng, K, Lin, Z, Uy, C, Yang, J, Chen, J, 2020. Biosens. Bioelectron. 155, 112064.
Zhu, J, Qian, J, Hou, X, He, J, Niu, X, Geng, W, Mu, J, Zhang, W, Chou, X, 2019. Smart Mater. Struct. 28 (9), 095014.
Zi, Y, Guo, H, Wang, J, Wen, Z, Li, S, Hu, C, Wang, Z L, 2017. Nanomater. Energy 31, 302–310.